Quaternary Science Reviews 291 (2022) 107655

Contents lists available at ScienceDirect

Quaternary Science Reviews

journal homepage: www.elsevier.com/locate/quascirev

Character of advance and retreat of the southwest sector of the British-Irish Ice Sheet during the last glaciation

Cristiana Giglio [a, *, 1], Sara Benetti [a], Ruth M.K. Plets [a, 2], Paul Dunlop [a], Colm Ó Cofaigh [b], Fabio Sacchetti [c], Elaine Salomon [a, 3]

[a] School of Geography and Environmental Sciences, Ulster University, Coleraine, BT52 1SA, Northern Ireland, UK
[b] Department of Geography, Durham University, Durham, DH1 3LE, UK
[c] Marine Institute, Rinville, H91 R673, Oranmore, Ireland

ARTICLE INFO

Article history:
Received 29 January 2022
Received in revised form
9 July 2022
Accepted 9 July 2022

Handling Editor: C. Hillaire-Marcel

ABSTRACT

Relict landforms and sediments across former glaciated settings provide information about ice-sheet dynamics and can contribute to the understanding of the behaviour of contemporary ice masses, for which observations are limited in spatial and temporal extent. In this study, we focus on the shelf offshore southwest Ireland, in the Celtic Sea, which was once occupied by the Irish Sea Ice Stream (ISIS), the largest ice stream draining the southern portion of the marine-terminating British-Irish Ice Sheet (BIIS). Newly acquired high-resolution multibeam echosounder, sub-bottom and core data enabled the investigation of the shelf geomorphology and of the sedimentology and chronology of glacial and glacimarine sediments. A suite of drumlins records ice sheet flow from the coastline towards the central part of the shelf in southwest Ireland. Pre-existing highs in the seafloor topography promoted the formation of arcuate and transverse landforms interpreted as a grounding-zone wedge and moraines and they document episodic retreat of the ISIS across this portion of the shelf. Observed lithofacies show consolidated subglacial till and laminated fine muds. The sediments provide evidence of ice grounded ca. 30 km off the south-west Irish coastline with subsequent deglaciation occurring under glacimarine conditions. These new data refine the current reconstructions of the dynamics of the southern BIIS. They reveal for the first time the interplay of marine- and land-based ice and the presence of grounded ice offshore SW Ireland. This study highlights the importance of high-resolution data in revealing palaeolandscapes as valuable analogues to test possible scenarios of modern ice sheet changes.

1. Introduction

Palaeo-ice sheet records, in the form of glacial landforms (e.g. drumlins, moraines) and sediments (e.g. glacial till and glacimarine deposits), yield direct evidence for past climate change by providing information on ice extent, flow dynamics and timing of advance and retreat (Stokes et al., 2015). Ice sheet reconstructions are therefore important for establishing the internal and external drivers that control ice sheet stability in a changing environment (e.g. Clark et al., 2000; Clark et al., 2009a, 2009b; Smith et al., 2020). Over the years, technological developments in marine geophysics and sediment sampling have been instrumental in the reconstruction of past ice sheets, especially of their marine-terminating margins, which can control overall ice-sheet stability. Ice streams, in particular, are integral components of the ice sheet-ocean-climate system. They are considered as ice-sheet arteries and fast-flowing corridors that are responsible for draining the ice sheet and regulating its mass balance and stability (Bennett, 2003; Rignot et al., 2011; Greenwood et al., 2021). Understanding the processes controlling ice stream flow is therefore critical to estimate future climatic scenarios (Price et al., 2011). This approach is vital given the current instability of the Greenland and Antarctic Ice Sheets in a warming world (Vaughan and Arthern, 2007; IPCC, 2021; Wood et al., 2021).

The last British-Irish Ice sheet (BIIS) was a marine-terminating

* Corresponding author. School of Geography and Environmental Sciences, Ulster University, Coleraine, BT52 1SA, Northern Ireland.
E-mail address: giglio-c@ulster.ac.uk (C. Giglio).
[1] Now at Green Rebel Marine Ltd, Crosshaven, Co. Cork, P43 EV21, Ireland
[2] Now at Vlaams Instituut voor de Zee (Flanders Marine Institute), Wandelaarkaai 7, 8400 Oostende, Belgium
[3] Now at School of Biological and Marine Sciences, University of Plymouth, Plymouth, PL2 8AA, UK

https://doi.org/10.1016/j.quascirev.2022.107655

and largely marine-based ice sheet (300,000 km^3; Fig. 1B and C) (Clark et al., 2012, 2018). Drained by ice streams and with one third of the volume of the present Western Antarctic Ice Sheet (WAIS), the BIIS represents a good analogue and candidate for palaeoglaciological studies of ice sheet responses to climate and ocean forcing (Clark et al., 2021). The southernmost sector of the last BIIS was drained by the Irish Sea Ice Stream (ISIS), the largest outlet to drain the former ice mass (Fig. 1B, C, D). Its size is comparable to some of the ice streams of the former Laurentide Ice Sheet (LIS) and the WAIS (Scourse et al., 2019). It has been suggested that topographic controls, internal glaciological mechanisms (i.e. overextension) together with relative sea-level rise, played an important role in controlling configuration changes in the BIIS through time (Smedley et al., 2017a, 2017b; Small et al., 2018; Bradwell et al., 2019; Davies et al., 2019; Callard et al., 2020; Van Landeghem and Chiverrell, 2020).

Although the latest research in the south of Ireland and its offshore sector by the BRITICE-CHRONO project provides a more refined picture of the maximum extent and deglaciation of this sector of the BIIS (Furze et al., 2014; Praeg et al., 2015; Lockhart et al., 2018; Scourse et al., 2019, 2021; Tóth et al., 2020), not all parts of the ISIS were investigated to the same level of detail. For example, the contribution of the ice in the south-western sector of Ireland to the advance and retreat of the last BIIS is still largely unknown. This is an important area of the ice stream, however, due to the potential interactions between the onshore-based Irish Kerry – Cork Ice Cap (KCIC) and the offshore E-W flowing ISIS (Ó Cofaigh and Evans, 2001a, 2001b; Ó Cofaigh and Evans, 2007; Ballantyne et al., 2011). Changes in bedslope and substrate geology close to the southern Irish coastline might have also caused differences in depositional behaviour between the centre and edges of the ISIS (Giglio et al., 2021), thus reflecting sensitivity of the ice to the bed characteristics across the Celtic Sea.

This study specifically investigates the geomorphological and sedimentary evidence of glacial and glacimarine environments on the south-western Irish shelf (Fig. 1B, D, 2). We achieve this by using ~3000 km^2 of already available high-resolution multibeam echo-sounder data, nine sediment cores and ~55 km of newly acquired sub-bottom data to reconstruct the spatial evolution of the palaeo-glacial landscape in this region. The results of this study offer new insights into the behaviour and direction of movement of the southern sector of the BIIS and provide new chronological constraints to its advance and retreat.

2. Regional setting and background

2.1. Study area

The Celtic Sea comprises the continental shelf offshore south of Ireland, the UK and northwest of France (Fig. 1A and B). The average depth of the shelf below sea level is around −100 m and it reaches up to −200 m towards the shelf-edge (Fig. 1B). The study area is located on the inner Celtic Sea shelf, ~30 km off the southwest coast of County Cork (Ireland; Fig. 1B). This area of the inner shelf is characterised by an elongated ENE to WSW-oriented bedrock topography (Fig. 2A). Where it crops out at the surface, particularly on the northern side of the study area, multibeam bathymetric and backscatter data reveal the cleaved and folded nature of the bedrock (Fig. 2A, C). This is the result of uplift and folding of Devonian and Carboniferous rocks (sandstone and mudstones) and related NE-SW-trending faults developed during the Variscan orogeny (McCann and Shannon, 1994; Pratch and Sleeman, 2002; BGS, 2013; GSI, 2014).

Relatively little sediment is preserved on the seabed close to the coastline and mostly as isolated patches of (sandy) mud or muddy sand, but the sediment drape over the bedrock becomes more consistent further offshore, where it is composed mostly of sands and gravels (Fig. 2D). At the seabed, glacial and glacially-related features are observed and their geomorphological mapping is provided in this study (Fig. 2B).

2.2. Previous work on the glacial history and regional stratigraphy of the Celtic Sea shelf

Approximately 27–25 cal ka BP, the Celtic Sea was occupied by the southernmost portion of the former BIIS, which extended onto the continental shelves of Ireland and the UK (Fig. 1B, C, D; Chiverrell et al., 2013; Praeg et al., 2015; Clark et al., 2018; Callard et al., 2018, 2020; Ó Cofaigh et al., 2019; Scourse et al., 2019, 2021). The Irish and Celtic Seas were occupied by the Irish Sea Ice Stream (ISIS), the largest ice stream to drain the interior of the BIIS, extending as far south as the Isles of Scilly and as far west as the shelf-edge (Fig. 1B) (Praeg et al., 2015; Smedley et al., 2017b; Scourse et al., 2021).

One of the first records of glaciation across the shelf was found in core 49/-09/44 recovered in the 1970s by the British Geological Survey (BGS) in the central part of the Celtic Sea (Fig. 1D). In this core, glacigenic sediments, referred to as Melville Till (MT), were directly overlayed by laminated glacimarine sediments, referred to as Melville Laminated Clay (MLC) (Scourse et al., 1990; Scourse and Furze, 2001). Analyses of vibrocores, retrieved in 2015 and 2019 from the shelf break (Fig. 1D), recorded stratified and overconsolidated diamict, interpreted as till, subglacially deposited by a grounded tidewater ice margin, which was overlayed by glacimarine muds resembling the Melville Laminated Clay (Praeg et al., 2015).

A calibrated radiocarbon age of 24.3 ± 1.2 cal ka BP from this laminated deposit (ibid.) provided a minimum age for glacimarine deposition and is consistent with the latest reconstructions of timing of ice maximum advance across the Celtic Sea between 27 and 24cal ka BP, ages determined in glacimarine sediments from a core transect across the shelf (Fig. 1D; Scourse et al., 2019). This timing also matches with a Bayesian analysis of onshore data suggesting a maximum ice advance across the shelf earlier than the previously discussed ages (Chiverrell et al., 2013). Collectively the recent reconstructions report that, by 25.6 ± 0.5 ka, the ice margin had reached its maximum extent at the shelf-edge, around 150 km farther seaward than previously thought based on core 49/-09/44 (Praeg et al., 2015; Smedley et al., 2017b; Scourse et al., 2019, 2021). This advance was rapid (300–600 m a^{-1}) and likely caused by overextension of the ice stream, characterised by thin ice progressing as a piedmont lobe from the topographic constriction of St George's Channel (Fig. 1B, D; Small et al., 2018). The surge-like behaviour resulted in a short-lived glacial advance to the continental shelf and pre-dates the global LGM (23–19 ka; Clark et al., 2009a, 2009b).

Evidence of ice rafting in cores from the Goban Spur and the Porcupine Seabight (Fig. 1B), together with dated glacimarine sediment close to the shelf-edge, suggest that deglaciation and initial pull-back of the ice margin was already underway by 25–24 ka BP (Van Rooij, 2004; Scourse et al., 2009; Haapaniemi et al., 2010; Praeg et al., 2015). The ice margin halted in the vicinity of St George's Channel at ~21 ka BP, possibly due to narrowing of the calving margin, resulting in a decrease in the rate of deglaciation at the time and the establishment of an oscillatory and dynamic margin (Small et al., 2018; Chiverrell et al., 2020; Coughlan et al., 2020; Van Landeghem and Chiverrell, 2020). ISIS dynamics are considered to be the result of a mix of external climatic controls (e.g. atmospheric temperature) acting during the initial phase of ice growth, and internal drivers, including bed-slope, underlying

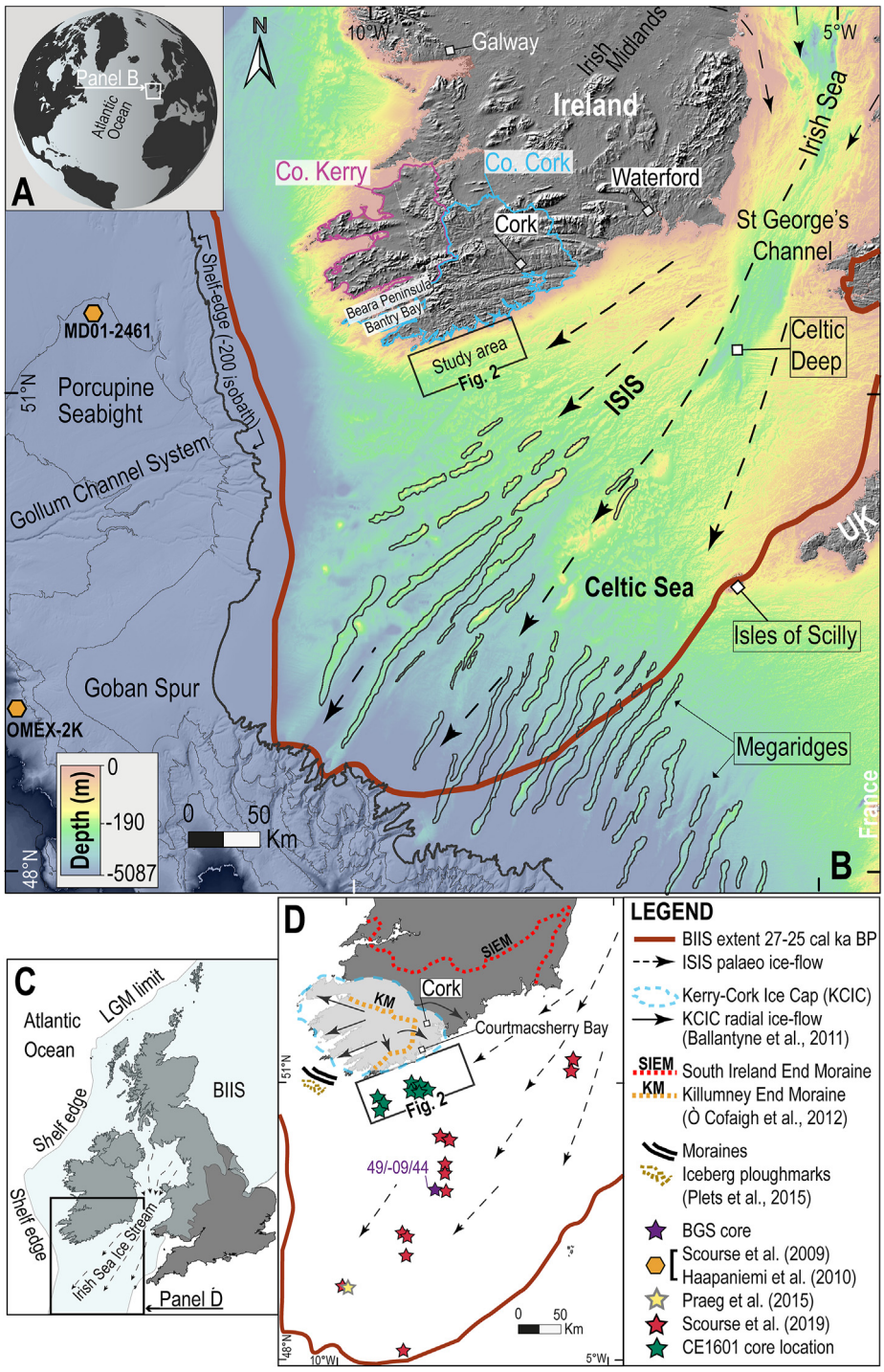

Fig. 1. Map of the study area. A) Global map of the area investigated in this study and located on the south-westernmost margin of Ireland and the UK (white box). B) Overview of the maximum extent of the British-Irish Ice Sheet (BIIS, thick red line) at c. 27-25 cal ka BP and related flow lines for its southernmost outlet known as the Irish Sea Ice Stream (ISIS) (Chiverrell et al., 2013; Praeg et al., 2015). Deep-sea cores MD01-2461 and OMEX-2K documented ice-rafted detritus (IRD) flux from the last BIIS (Scourse et al., 2009; Haapaniemi et al., 2010). The location of the study area is indicated together with onshore and offshore key locations. Co. = County; C) The maximum extent of the BIIS during the LGM (Chiverrell and Thomas, 2010; Clark et al., 2012). D) Data from previous works, as discussed in section 2. BGS core 49/-09/44 recovered glacigenic sediments of the Melville Till (MT) and Melville Laminated Clay (MLC) (Scourse et al., 1990). Core locations discussed in Scourse et al. (2019) and Praeg et al. (2015) documented the glacigenic sequences across the Celtic Sea shelf and timing of the ISIS advance across and retreat from the shelf. The approximate location of moraines (longer black lines) and iceberg scours (shorter brown lines) are reported from Plets et al. (2015) that tentatively propose these marks as linked to the retreat and calving of the local Kerry– Cork Ice Cap (KCIC). The location of the study area (black box) and related sediment cores (green stars; CE1601) offshore the south-west Irish sector are also shown. (For interpretation of the references to colour in this figure legend, the reader is referred to the Web version of this article.)

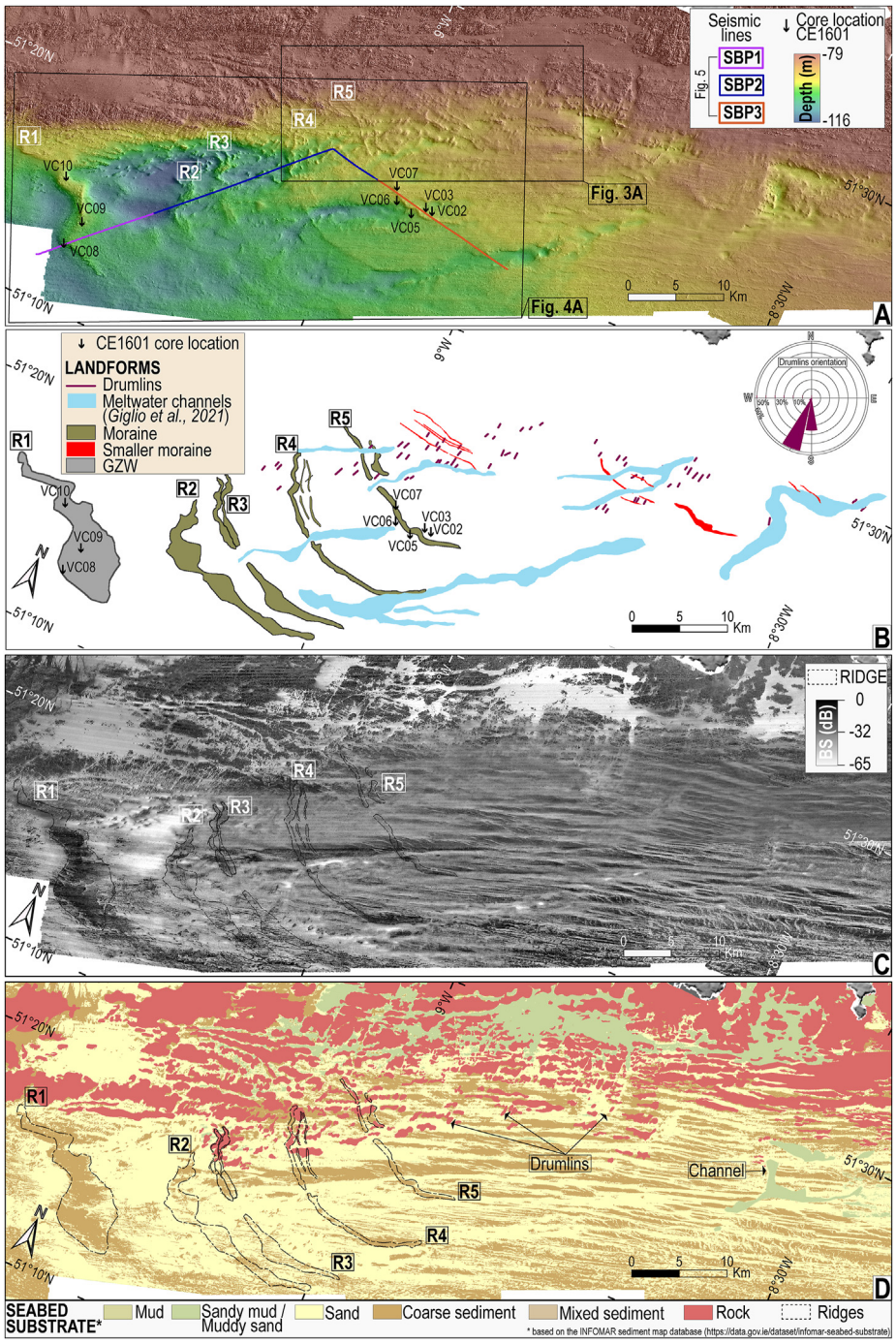

Fig. 2. A) Bathymetry of the study area with the location of the ridges (R1 to R5 and eastern smalle'r ridges), sub-bottom profiles (SBP1 to SBP3) and the sediment cores (CE1601, VC02 to VC10) analysed in this study. B) Geomorphological map of glacial and glacially-related landforms. The rose diagram at the top right refers to the orientation of drumlins. GZW = Grounding Zone Wedge. C) Backscatter (BS) data for the study area coupled with D) the INFOMAR Seabed Substrate map for the same area. The different sediment types are based on acoustic classes extracted from the backscatter strength and analysis on grab-samples (https://data.gov.ie/dataset/infomar-seabed-substrate). Sediment classes are based on a modified Folk classification and coarse sediment includes gravelly sand, sandy gravel and gravel, whilst mixed sediment includes muddy gravel, gravelly mud and mixes of mud, sand and gravel in different proportions.

geology and bedrock topography, mostly affecting rate and pattern of deglaciation (Smedley et al., 2017a; Small et al., 2018; Chiverrell et al., 2020; Scourse et al., 2021).

Along the south-east coast of Ireland, the interaction between inland ice and the ISIS is recorded in raised beach deposits dating back to MIS4-3, that are intermittently exposed onshore in the 'Courtmacsherry Formation' (Fig. 1D; Wright and Muff, 1904; Greenwood and Clark, 2008; Ó Cofaigh et al., 2012a, 2012b). Above this Formation, the ISIS deposited during MIS2 a subglacial till, known as the Irish Sea Till (IST). This unit is described as a massive, fine-grained, shelly diamict. Radiocarbon dating derived from shells reworked into the IST constrained a maximum age of ~24 cal ka BP for the ISIS advance towards the shelf (Ó Cofaigh and Evans, 2001a; 2001b, 2007). In the recent Bayesian model by Scourse et al.

(2021), this age post-dates the ice maximum extent on the shelf around 25.6 ± 0.5 ka BP. Hence, the IST was re-interpreted as diamict deposited during oscillatory retreat of the ISIS margin across south and southeast Ireland (Scourse et al., 2021). The correlation with the regional stratigraphy of the Celtic Sea denotes that MT and MLC are the offshore equivalent of the IST, as they represent the ISIS depositional events during the last glacial period (Evans and Ó Cofaigh, 2003). Further retreat of the ISIS from the southern Irish coastline is indicated by the presence of glaciolacustrine sediments (fine sand and gravel beds) exposed on land and overlying the IST. These glaciolacustrine sediments are interpreted as deglacial outwash, from which a suite of Optically Stimulated Luminescence (OSL) ages range between 24.4 ka and 21.6 ka (Ó Cofaigh et al., 2012a, 2012b). The glaciolacustrine deposits are in turn overlain by till deposited by inland ice flowing from the Irish Midlands across ground previously occupied by the ISIS (Ó Cofaigh et al., 2012a, 2012b). Inland ice advance likely reached more than 15 km beyond the present coastline (Tóth et al., 2020).

Whilst offshore southern Ireland was occupied by the ISIS, the mountains of SW Ireland remained under the influence of the Kerry-Cork Ice Cap (KCIC, Fig. 1D; Ballantyne et al., 2011). The ice cap constituted an independent centre of ice dispersal flowing west over the peninsulas of west Kerry and, during the last glacial period, was coalescent with ice from the Irish midlands to the east and with ice from Galway to the north (Fig. 1B, D; Ballantyne et al., 2011; Clark et al., 2012). The northern and eastern lateral extent of the KCIC is marked by the Kilumney End Moraine (KM; Fig. 1D). Different interpretations with regard to the timing of formation of this morainic ridge exist. These include an LGM limit or a post-LGM readvance (for discussion refer to Ballantyne et al., 2011), or a recessional moraine alongside the South Ireland End Moraine (SIEM) formed during the last deglaciation (Fig. 1D; Ò Cofaigh et al., 2012a, 2012b). The deglaciation of the KCIC is also not well defined: two 36Cl dates from low grounds south of Bantry Bay (Sheep's Head Peninsula; Fig. 1B) indicate ages of 22.0 ± 3.4 and 21.3 ± 1.3 ka for ice-free conditions (Bowen et al., 2002). However, cosmogenic nuclide inheritance issues have been suggested for these dates as more recent works indicate deglaciation of the local ice cap after 19 ka (for discussion refer to Clark et al., 2012).

In addition, the KCIC appears short-lived and its offshore extent remains speculative. Evidence from ice-abraded bedrock slabs from the Beara Peninsula indicates that this area was entirely covered by ice of Kerry-Cork provenance, with ice thickness exceeding 700 m across the local mountain summits in the area (Fig. 1B, D; Ballantyne et al., 2011). Based on this information, Ballantyne et al. (2011) concluded that the KCIC extended offshore during the LGM. Currently no widespread evidence exists to corroborate this interpretation. However, iceberg ploughmarks were detected in shallow water (max. 100 m) close to the current coastline of Bantry Bay and tentatively linked to the retreat and calving of the local KCIC (Fig. 1B, D; Plets et al., 2015). To the east of the iceberg scours, closer inshore, large linear ridges have been mapped and tentatively interpreted as retreat moraines attributed to the ice cap (Fig. 1D). If this were the case, the KCIC would have extended at least ~20 km offshore of Bantry Bay. However, such a scenario is in contrast with previous interpretations of the KCIC as composed of valley glaciers (Clark et al., 2012). Therefore, to date, the offshore extent of the KCIC cannot be delineated with certainty and there is no evidence for its potential interaction with the ISIS offshore southwest Ireland.

3. Material and methods

3.1. Geophysical data

This study uses multibeam echo-sounder (MBES) bathymetry and backscatter data collected by the Irish Marine Institute, as part of the INFOMAR (INtegrated Mapping FOr the Sustainable Development of Ireland's MArine Resource) Programme, and sub-bottom data collected by Ulster University during research cruise CE21015. INFOMAR MBES data were acquired between 2012 and 2016 onboard the R.V. *Celtic Voyager* using hull-mounted, high-resolution Kongsberg Simrad EM 2040 (200–400 kHz) and EM3002 (300 kHz) systems following international hydrographic standard practice IHO S-44 1a (IHO, 2020). Integrated GNSS/L-Band receiver CNAV 3050 was used for primary position corrections (horizontal/vertical accuracies of ±10 cm) with a Seatex Seapath 330+ acting as a secondary positioning system and providing motion referencing and timing. Sound velocity profiles for refraction corrections were acquired with an AML SvPlus SVP and real-time AML surface sensor. Data quality control indicated compliance with IHO Order 1a standard (IHO, 2020). Bathymetric and backscatter data were processed and cleaned by the Irish Marine Institute using the hydrographic package CARIS Hips & Sips and QPS FMGT Geocoder, respectively. The multibeam grids were subsequently delivered at 5 and 10 m resolution and exported as rasterised digital elevation models (DEMs) in ellipsoid WGS84 UTM 29 N projection. Analysis of the resulting multibeam data was performed in ESRI ArcGIS 6.10, where mapping of glacial and glacially-related features was achieved by onscreen digitising (e.g. Jakobsson et al., 2016). Multidirectional oblique-weighted hillshade visualisations were generated from the DEMs with no vertical exaggeration to map and interpret the geomorphological features identifiable on the bathymetric data. Polygon or polylines shapefiles were produced to outline the landforms on their break of slope, compared to the surrounding seafloor. Within ArcGIS, semi-automatic tools (i.e. Intersect, Stack Profile) were applied to record heights, lengths and widths together with the construction of topographic profiles for the digitised landforms. The preferred direction of the streamlined mounds was calculated based on their long-axis orientation. Information on bedrock and sediment distribution on the seafloor was extracted from the INFOMAR Seabed Substrate map layer obtained through the open access portal https://data.gov.ie/dataset/infomar-seabed-substrate.

During research cruise CE21015 in 2021 on the R.V. *Celtic Explorer*, sub-bottom data were acquired to provide information on acoustic stratigraphy and sediment thickness. The location of the sub-bottom profiles was chosen based on the distribution of mapped landforms and core locations to achieve maximum coverage in the limited time available for data collection. The system used was a hull-mounted iXblue Echoes 3500 Chirp operating at 1.7–5 kHz. Pre-processing was carried out onboard with the DELPH Interpretation software used to perform heave correction and conversion into SEG-Y files. Post-processing was carried out using IHS Kingdom and involved trapezoid band-pass filtering (1.8-2.0- 6.0- 6-2 kHz), Automatic Gain Control (AGC at 10, 30, 50 and 70 ms) and wavelet envelop calculation on the previously performed AGC. Seismic depths have been converted from two-way travel time (s) to metres (m) using an acoustic interval velocity of 1650 ms^{-1} estimated based on studies from similar geomorphological settings in the Celtic Sea shelf and adjacent areas (Plets et al., 2015; Lockhart et al., 2018; Tóth et al., 2020). Following the seismic interpretation, the drawings were finalised in Adobe Illustrator for clarity.

3.2. Sediment cores

Nine sediment cores (Figs. 1 and 2A, B, 4, Table 1) were collected by the INFOMAR programme onboard the R.V. *Celtic Explorer* in 2016 (CE1601) around two morphological ridges (R1 and R5; Fig. 2A and B), identified from the MBES data. A GeoResources vibro-coring system was used with 6 m liners and an internal diameter of 10 cm. Core recovery was between 0.25 and 4.60 m (Table 1). Cores were cut into 1 m sections and are stored in a refrigerated facility (+4 °C) at Ulster University. The cores were split in halves and subsequently photographed, visually described and strength measurements were made at 20 cm intervals with a handheld Torvane. A CARETSRAEM DRX- Evolution System scanner from the School of Radiology (Jordanstown campus, Ulster University) provided X-ray images on the split cores to further refine the core lithofacies.

Six samples for radiocarbon dating were selected as 1–2 cm slabs (Table 2), usually targeting the boundaries between glacial, glacimarine and post-glacial deposits. Each sample was wet-sieved on a 63 μm sieve and dried under infrared lamps. Single valves or benthic foraminifera samples were dry-picked using an Olympus SZX16 binocular microscope, mainly in the fraction ≥125 μm to obtain enough material for dating. Samples were prepared and analysed for ^{14}C at the Scottish Universities Environmental Research Centre Accelerator Mass Spectrometry (AMS) laboratory (SUERC publication code) or the Keck Carbon Cycle AMS Facility, University of California, Irvine, USA (UCIAMS publication codes, Table 2). Ages derived from diamicton interpreted as subglacial till were based on reworked shell material. They provide a maximum age on till formation and thus constrain the onset of ice-sheet advance across the shelf. Conversely, samples taken from glacimarine sediments above the diamicton represent conditions free from grounded ice and thus yield a minimum age of retreat. The conventional radiocarbon ages were calibrated using the globally averaged marine calibration curve (Marine 20), with an inbuilt marine reservoir correction of 400 years and $\Delta R = 0$ (Calib v.8.2.0., Heaton et al., 2020), following the protocol recently established by the BRITICE-CHRONO project (Callard et al., 2018, 2020; Scourse et al., 2019, 2021; Benetti et al., 2021; Ó Cofaigh et al., 2021). This allows for chronological correlations to be made between the findings in this paper and previously published dates for the southern sectors of the BIIS (Furze et al., 2014; Lockhart et al., 2018; Scourse et al., 2021). Dates are reported in Table 2 as 2σ range calibrated years before present (cal yr BP) unless otherwise stated.

Five cores (VC02, VC03, VC05, VC06 and VC08; Fig. 2A) were sub-sampled as 1 cm thick slabs for micropalaeontological analysis. Subsamples were collected to gain information on foraminifera assemblages and confirm the environmental conditions of specific facies (Murray, 2006). Three cores (VC02, VC03, VC05) were sampled at 20 cm intervals through the entire core length and additional two cores (core catchers of VC06 and VC08) were sampled at specific core-depth to support the lithofacies interpretation. The samples were wet-sieved on a 63 μm sieve to remove the mud fraction and subsequently dried under infrared lamps. A Green Geological microsplitter was used to split the samples into aliquots that contain ≥300 specimens of benthic foraminifera. Foraminifera were picked from the 150–500 μm size fraction using an Olympus SZ51 binocular microscope. Only benthic foraminifera were identified to species level (where possible) according to Murray (2003), Hanagata and Nobuhara (2015) and Clark and Patterson (1993). Total species counts were then converted to percentages, including planktonic species. Foraminifera density was calculated as the number of individuals per gram dry-bulk weight sediment (Peters et al., 2020). Fisher's α diversity index on benthic foraminifera refers to the counts of individuals and their abundances within a sample (Fisher et al., 1943).

4. Results and interpretations

In this section, the description and interpretation of the landforms from multibeam and sub-bottom profiler data are followed by analysis of sediment cores and their interpretation in terms of depositional processes.

Table 1
Details of the core location, water depth and recovered length.

Cruise – Core no.	Latitude (N)	Longitude (W)	Water depth (mbsl)	Core length (m)
CE1601 – VC02	51°20′59.9″	8°55′6.4″	99	0.25
CE1601 – VC03	51°21′15.5″	8°55′28.9″	99	2.28
CE1601 – VC05	51°20′45.8″	8°56′13.2″	99	1.67
CE1601 – VC06	51°21′2.4″	8°57′32.0″	99	1.19
CE1601 – VC07	51°21′33.48″	8°58′7.53″	99	1.14
CE1601 – VC08	51°12′59.8″	9°17′36.9″	98	2.14
CE1601 – VC09	51°14′13.9″	9°17′8.16″	97	2.90
CE1601 – VC10	51°15′45.2″	9°19′30.6″	98	4.60

Table 2
Radiocarbon samples and related ages for the cores discussed in this study.

Publication code	Core (CE1601)	Sample depth (cm bsf)	Sample type	Lithofacies	^{14}C Age (yr BP) ± 1σ	Calibrated age (cal yr BP) ± 2σ ΔR = 0 yr
UCIAMS-251324	VC03	41–42	Gastropod	Friable diamicton (Dmm)	8770 ± 180	9241 ± 488
SUERC-97280	VC03	52–54	Single shell fragment – *Venus Casina* (Linnaeus, 1758)	Laminated mud (Fl) ?	7512 ± 38	7789 ± 145
SUERC-97284	VC05	66–68	Bivalve shell, *Timoclea ovata* (Pennant, 1777)	Friable diamicton (Dmm)	9064 ± 38	9582 ± 165
UCIAMS-251325	VC05	81–82	Mixed benthic foraminifera	Laminated mud (Fl)	11030 ± 60	12381 ± 245
SUERC-97285	VC05	146–148	Multiple shell fragments	Subglacial till (Dmm_c)	37239 ± 509	41082 ± 772
SUERC- 97286	VC06	100–103	3 valve shells, *Glycimeris glycimeris* (Linnaeus, 1758)	Friable diamicton (Dmm)	9088 ± 38	9609 ± 174

4.1. Seabed geomorphology from multibeam data

4.1.1. Streamlined landforms

A field of ~65 linear to oval streamlined hills are observed (Fig. 3A, C, D), north-east of a set of ridges (section 4.1.2). The streamlined landforms are found in clusters and arranged in a belt-like configuration, which results in a small corridor running W-E and, thus, parallel to the coast in water depths between −84 and −108 m (Fig. 2A and B, 3A, C, D). The long-axes or crests of the mounds are SSW-oriented and on average 390 m long (Figs. 2B and 3C, D, S1A). The mounds are between 0.9 m and 3 m high compared to the surrounding seafloor, they tend to be 100–150 m wide with corresponding mean elongation of 3.2 (Fig. S1A). Generally, the individual morphology of the mounds exhibits a stoss- and lee-side, resulting in a streamlined appearance of the seabed. They tend to be asymmetric in the sense that they are higher and wider

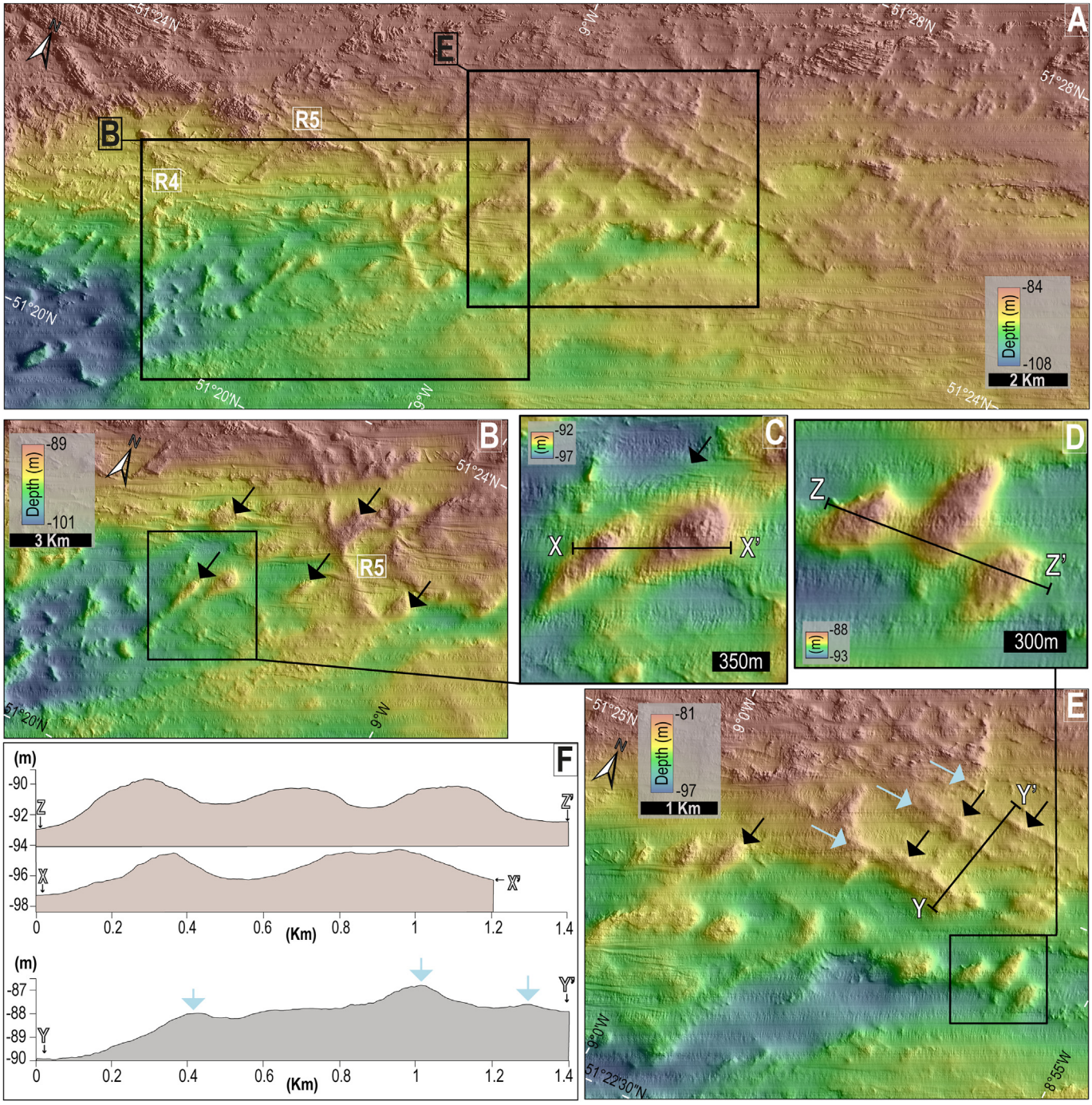

Fig. 3. A) Overview of the bathymetric data in the north-east of the study area, as indicated in Fig. 2A. B) Streamlined mounds interpreted as drumlins. The black arrows indicate the direction of the mounds' long-axes. C, D) Representative drumlin examples observed in the study area. E) Slightly reworked drumlins (black arrows) overprinted by the small-sized, closely-spaced ridges interpreted as recessional moraines. For the latter, the light blue arrows indicate the position of ridge profile. These small-sized ridges are oriented WNW-ESE. F) Topographic profiles of the drumlins (X-X′ and Z-Z′) and moraines (Y–Y'; light blue arrows indicate the position of the ridges). (For interpretation of the references to colour in this figure legend, the reader is referred to the Web version of this article.)

towards the coastline and taper in the offshore direction (Fig. 3C and D). In places, they have been overprinted by the ridges described in the following section (Fig. 3E).

4.2. Large arcuate and small sinuous ridges

Multibeam bathymetric data show a series of five ridges at water depths between −90 m and −116 m. They appear arcuate, aligned and slightly concave in planform (Figs. 2B and 4). The ridges are characterised by a convex-seaward geometry and their long-axes have prevalent NW-SE orientations. The westernmost ridge 1 (R1; Fig. 4A and B) can be traced horizontally for approximately 1600 m. In planform, R1 is concave, wedge-shaped, between 380 and 4900 m wide and with en echelon crest segments ~9 m high. This makes it the most prominent of all ridges (Figs. 2B and 4B, S1B, Table S1). Three of the cores were collected from R1 (VC08, VC09, VC10; Fig. 2A and B, 4A, 7).

R2 is located 6500 m to the east of R1 (Figs. 2B and 4A). It has the same NW-SE orientation, is ~1800m long, ~5 m high and varies in width between 360 and 2500 m (Fig. 4A, S1B, Table S1). The southern end lacks a distinctive break in slope and blends into the local topography. A few kilometres to the northeast, R3 has a composite morphology, as its northern end is bifurcated into two smooth parallel crest lines between 700 and 1100 m long (Fig. 4A, S1B, Table S1). R3 is between 230 and 1500 m wide, 1−3 m high and it is cut by a channel crossing this portion of the shelf (Figs. 2B and 4A, S1B, Table S1). About 5 km further north, R4 and R5 are found ~8 km apart. Both have an NNW-SSE orientation and are again crossed by channels (Figs. 2B and 4A, C). R4 is on average 400 m wide, ~1800 m long and between 3 m and 5 m high (Fig. 4A, S1B, Table S1). Directly behind the ridge, two smaller ridges (~5000 m long, 1−2 m high and around 120 m wide) are also visible and form part of R4. R5 is the last of the sequence; it is ~1900 m long in total, on average 400 m wide and between 3 and 7 m high (Fig. S1, Table S1). Five cores were collected near R5 (VC02, VC03, VC05, VC06, VC07; Fig. 4A). The cross-sectional profile (J-J′-J″) shows that all the ridges, from R1 to R5, are sharp-crested and relatively symmetric with gentle proximal and distal slopes. R1 is largest and more asymmetric, with a steeper shelf-facing side and gentler coastline-facing slope (Fig. 4A and B).

A number of smaller, closely-spaced, parallel to sub-parallel, linear to curvilinear ridges are also observed at around −90 m water depth, some 5 km eastward from R5 (Figs. 2B, 3E and 4C in light blue). They are evenly spaced (<800 m apart) and occur in a cluster with a preferential WNW-ESE orientation. These ridges are sharp-crested, symmetric with gentle proximal and distal slopes. They vary in length between 200 and 10,000 m, are on average 500 m wide and 2 m in height and are thus smaller compared to R1-R5 (Fig. 3E). Both the arcuate, prominent landforms described above and these linear to curvilinear ridges are superimposed onto the streamlined mounds (section 4.1.1; Figs. 3E and 4C).

The backscatter signature over R1 is higher compared to the slightly lower backscatter intensity across the other ridges and surrounding areas (<−32 dB; Fig. 2C) suggesting the presence of coarser material and finer sediments, respectively (Fig. 2D). The other ridges do not display distinct backscatter patches, but cross the area mapped as widespread sand with ribbons of coarser sediments (Fig. 2D). The area between R1 and R2 shows a clear pocket of low backscatter intensity, also corresponding to the deepest seafloor in the area (−116 m; Fig. 2A), suggesting the interior is filled with finer sediment (Fig. 2D).

4.3. Seabed geomorphology interpretation

In terms of morphology, the streamlined mounds resemble similar features observed and mapped elsewhere on the UK and Irish continental shelves and on other formerly or presently glaciated continental margins (Fig. S1A; Smith et al., 2007; Benetti et al., 2010; Dunlop et al., 2010; Jónsson et al., 2014; Dove et al., 2015; Ó Cofaigh et al., 2019; Sookhan et al., 2021; Szuman et al., 2021b). Typical lengths for streamlined features are generally between 100 and 1000 m, with widths three times smaller (Clark et al., 2009a, 2009b). These measures are consistent with the morphometry of the streamlined mounds on the inner shelf (Fig. 2B, Table S1).

Table 3
Acoustic facies examples identified in the sub-bottom profile data in the shelf offshore southwest Ireland, in the Celtic Sea, with associated lithofacies from cores CE1601. For lithofacies codes refer to section 4.3 or lithofacies summary in Table 4.

Acoustic Facies (AF)	Sub-bottom Example	Description	Interpretation	Corresponding lithofacies (as in Fig.7)
AF1	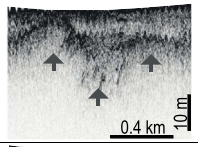	Rugged basal reflector (see grey arrowed reflector, also in AF2) and is acoustically structureless below this reflector.	Bedrock	
AF2	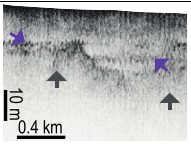	Acoustically semi-transparent with weak discontinuous reflections. Ranges in morphology and it includes large ridges, small mound, asymmetric wedges and stacked sheets.	Till sheets, drumlins, GZW, and moraines. Glacial to proximal/distal glacimarine sediments.	Fm Fl Dmm$_r$ Dmm Dmm$_c$
AF3	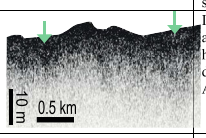	Internally structureless and acoustically homogeneous. Forms a discontinuous drape onto AF2.	Outwash sediments, coarse glacimarine deposits.	Gfu Gms
AF4	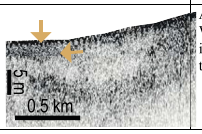	Acoustically transparent. When AF3 is absent, it infills depressions at the top of AF2.	Post-glacial basin fill.	Suf$_2$ Suf$_1$

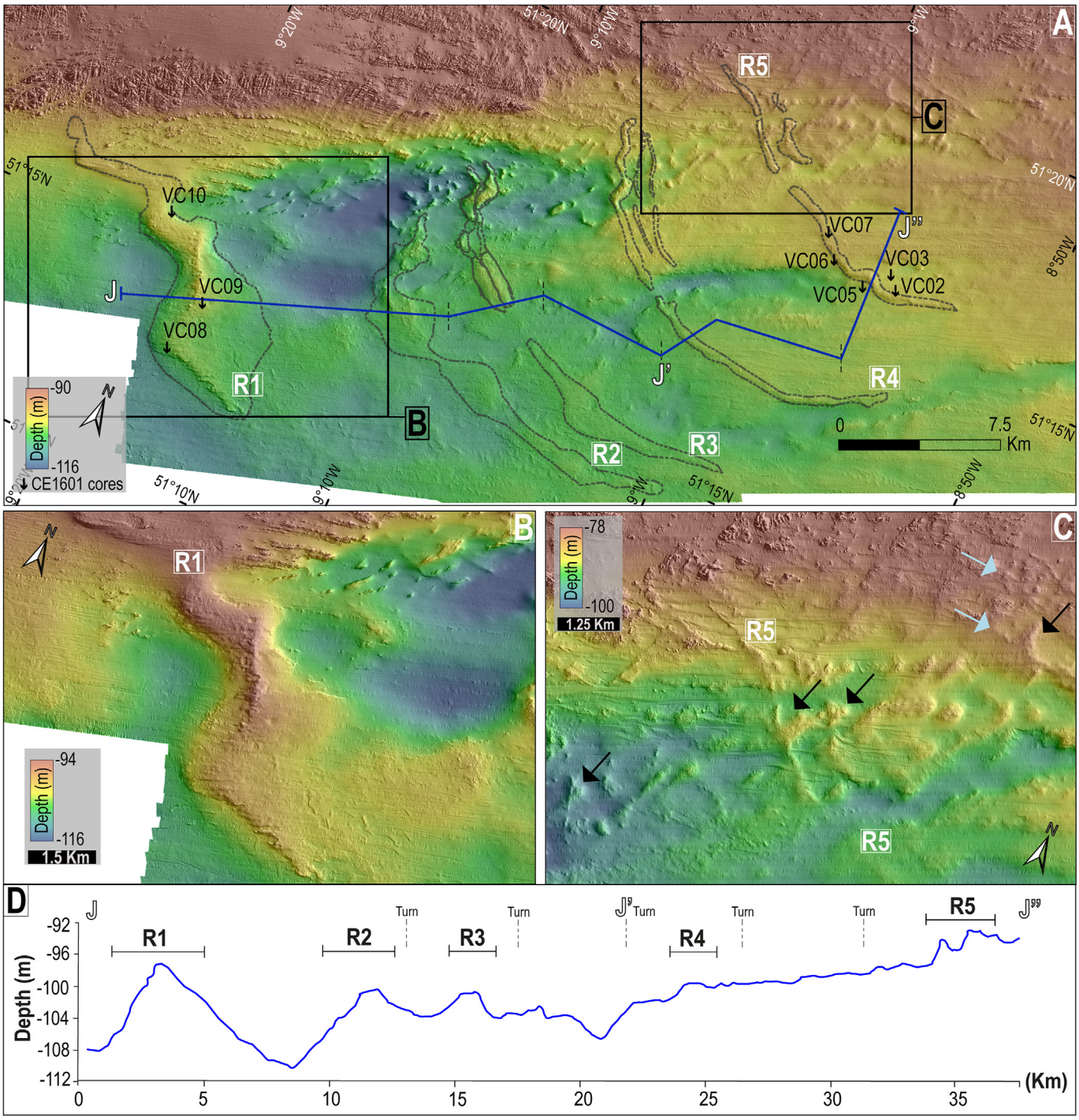

Fig. 4. A) Bathymetry in the area of the arcuate ridges (R) delineated by dotted areas; the black arrows indicate the locations of sediment cores (Table 1). The vertical dashed lines on the profile J-J′-J″ indicate the turns reported in panel D. B) Close-up of R1, the largest and most continuous in the sequence of ridges. C) Detail of R5 and smaller ridges (light blue arrows) superimposed on the streamlined mounds (black arrows). D) The bathymetric profile J-J′-J″ crosses the sequence of ridges, with R1 showing a more asymmetric profile with a steep seaward side and a more gentle landward side. R2 to R5 are more symmetric and shorter in size. For detailed site location and core coordinates see Fig. 2A and Table 1. (For interpretation of the references to colour in this figure legend, the reader is referred to the Web version of this article.)

Because of this resemblance, we interpret these landforms as drumlins, which are formed subglacially.

The direction of the drumlins' long axis is parallel to the direction of ice flow (e.g. Benn and Evans, 2010; Iverson et al., 2017). Owing to their association with ice flow (Jamieson et al., 2016; Livingstone et al., 2016; Stokes, 2018), drumlins are a key element for the identification of palaeo-ice streams in both terrestrial and marine settings (Szuman et al., 2021a). The drumlins on the Celtic Sea shelf are oriented SSW thus recording south-westerly ice flow across the shelf at the time of their formation (Figs. 2B and 3B, C, D).

The prominent arcuate R1 is interpreted as a grounding-zone wedge (GZW) (Batchelor and Dowdeswell, 2015; Simkins et al., 2018; Bradwell et al., 2019; Greenwood et al., 2021). This GZW is similar in size and morphology to those found on the previously

glaciated UK and Norwegian shelves (Ottesen et al., 2005; Shipp et al., 2002; Callard et al., 2018) and in modern Antarctic regions, such as the Larsen continental shelf (Dowdeswell and Fugelli, 2012; Evans and Hogan, 2016). GZWs are typically oriented perpendicular to the direction of ice flow and display an asymmetric profile. They reflect temporary halts of the ice margin during overall retreat, promoted by the presence of underlying topographic highs (Lønne, 1995; Batchelor and Dowdeswell, 2015). The rate of this retreat, together with sediment flux, controls their dimension (Dowdeswell and Fugelli, 2012). They are associated with gravity-flow processes and the delivery of subglacial diamict to the ice margin (Powell and Alley, 1997).

The lower (max. 7 m) and slightly concave R2 to R5 ridges and the closely-spaced, smaller ridges located north-east of the larger ridges (Fig. 3B, E, 4A, C) have the typical morphology of moraines (e.g. Schomacker, 2011). Together, these clustered ridges likely represent ice marginal and recessional moraines that are often formed by still-stand or minor (e.g. seasonal) ice margin re-advances during an overall retreat phase (Batchelor and Dowdeswell, 2015). Such a clustered character and linear or concave morphology are typical of moraines formed at grounded tidewater ice cliffs (Ottesen et al., 2017; Dowdeswell and Fugelli, 2012).

The relatively good preservation of the GZW and moraines on the seafloor and the fact that they overprint the drumlins suggest that the ridges are related to the final stages of ice movement across the area. A series of channels, interpreted as meltwater channels, are cross-cutting the moraines almost perpendicularly, indicating a later meltwater erosional event (Giglio et al., 2021).

4.4. Shallow acoustic facies and seismic stratigraphy

Based on the sub-bottom profiler data, we define four acoustic facies, AF1-AF4 (Table 3). AF1 is the deepest unit imaged in the sub-bottom data and represents the acoustic basement in the study area. It has an impenetrable character with lack of internal reflections except towards the east of the study area where some south-eastward dipping reflectors are observed (SBP1, SBP3, Fig. 5C and D, Table 3). AF1 has a discontinuous upper surface reflector of high to medium amplitude and it has usually a rugged appearance (Fig. 5D).

AF2 is acoustically semi-transparent with weak discontinuous reflections. It is bounded by the high to medium amplitude reflector of AF1 at the base and it fills the deepest troughs of AF1. The top bounding surface is a mostly continuous, relatively high amplitude reflector that varies between irregular to smooth. AF2 reaches its maximum thickness (~20 m) across R1 and it thins eastward where it displays a sheet geometry in SBP3 (Fig. 5C and D). AF2 is continuously mapped across the study area including below the GZW, moraines and drumlins (as detected on the multibeam data) and was recovered by four cores adjacent to R1 and R5 (Fig. 5A, B, C). Some channels occur within this facies: they are mostly infilled with sediment and channel depths range between 5 and 20 m. In the areas where drumlins have been interpreted from the bathymetry, the sub-bottom profiles indicate that these are substantially taller (5–8 m high) than visible on the seabed topography. AF2 was penetrated with three cores (VC03, VC05 and VC06) near R5 and one core (VC08) on top of R1.

AF3 is internally structureless and acoustically homogeneous (Table 3). The upper surface is bounded by the seabed while the lower surface drapes over the high amplitude surface reflector of AF2 (Fig. 5D). This facies forms a discontinuous drape that reaches a thickness of ca. 2 m in most places with a maximum of 5 m on top of R1. AF3 was recovered in four cores (VC10, VC09, VC07 and top of VC08; Figs. 4 and 5).

AF4 is acoustically transparent and, where AF3 is absent, the seabed reflection represents the upper boundary of AF4 (Fig. 5D, Table 3). The facies itself consists of discontinuous reflectors; it infills depressions visible at the top of AF2 and it was ground-truthed in all of the cores in the area.

4.5. Shallow acoustic facies and stratigraphic interpretation

AF1 is the acoustic basement of the area, acoustically structureless below the basal reflector with a rugged appearance and occasionally with south-eastward dipping reflectors. AF1 is interpreted as the bedrock and likely correspond to the Devonian and Carboniferous rocks outcropping in the northern part of the study area and dipping in the direction of the central Celtic Sea shelf (Fig. 2A, C, D, 5D). Where AF1 crops out at the seafloor, the multibeam and backscatter data reveal a similar rugged topography and hard substrate compared to the surrounding area that further support our interpretation.

AF2 is the thickest across the area (up to 20 m) and comprises the infill of the basins of AF1, as well as the large ridge corresponding to the topographic high of R1, together with a series of moraines, drumlins and possible channels (visible in SBP2 and SBP3 in Fig. 5B, C, D). AF2 was sampled in four cores recovering laminated mud overlying compact diamicton (VC03, VC05), massive mud (VC08) and compact diamicton (VC06) (see section 4.3; Fl, Fm and Dmm_c; Figs. 5 and 7). Therefore, this unit is interpreted to be glacial to glacimarine in origin and deposited during advance and retreat of the ice margin onto the shelf. Some channels interpreted as meltwater channels (Giglio et al., 2021) are found cut into and infilled by AF2 and they account for cross-cutting the morainic ridges at the seafloor.

AF3 is found draping AF2 and was sampled in four cores recovering between 2 and 4.8 m in total of moderately sorted, clast-supported gravel (see section 4.3; Gms, Gfu; Figs. 5 and 7). The acoustic properties, together with the sediment cores, suggest that AF3 is made up of glacial outwash sediments deposited in a glacimarine system (Rust and Romanelli, 1975; Benn and Dawson, 1987). The presence of meltwater channels may also be consistent with the deposition of AF3 in a subaqueous environment (Powell, 1990). AF3 reaches a maximum thickness of 5 m on top of R1. Here the high backscatter return supports the classification of the deposit as coarse sediments (Fig. 2C and D).

AF4 corresponds to the uppermost unit, and it is interpreted as post-glacial basin fill. This unit was recovered at the top of all the cores, comprising coarse-grained sand with abundant biogenic material, including whole shells. These characteristics combined with the stratigraphy are consistent with post-glacial sediment deposited by bottom-current winnowing in an open marine environment (Viana et al., 1998; Stow et al., 2009).

4.6. Lithofacies description and micropalaeontology

Eight lithofacies were identified in the sediment cores (Figs. 6 and 7 and Table 4). The lithofacies codes are based on the classification system from Eyles et al. (1983).

Lithofacies Dmm_c is a compact (58 kPa), massive, matrix-supported diamicton, found at the base of three cores (228-224 cm in VC03, 167-141 cm in VC05 and 120-105 cm in VC06; Fig. 7). It is a very dark, greyish brown to dark grey (Munsell colour 2.5Y 4/2, 2.5Y 3/2) diamicton with sub-angular to sub-rounded pebbles and grains and the clast lithologies vary from magmatic to sedimentary and metamorphic. Clast alignments and sedimentary structures (e.g. stratification, dewatering structures) within the diamict are absent and not evident on the X-radiographs either (Fig. 6). Facies thickness ranges between 4 cm up to 20 cm (Fig. 7).

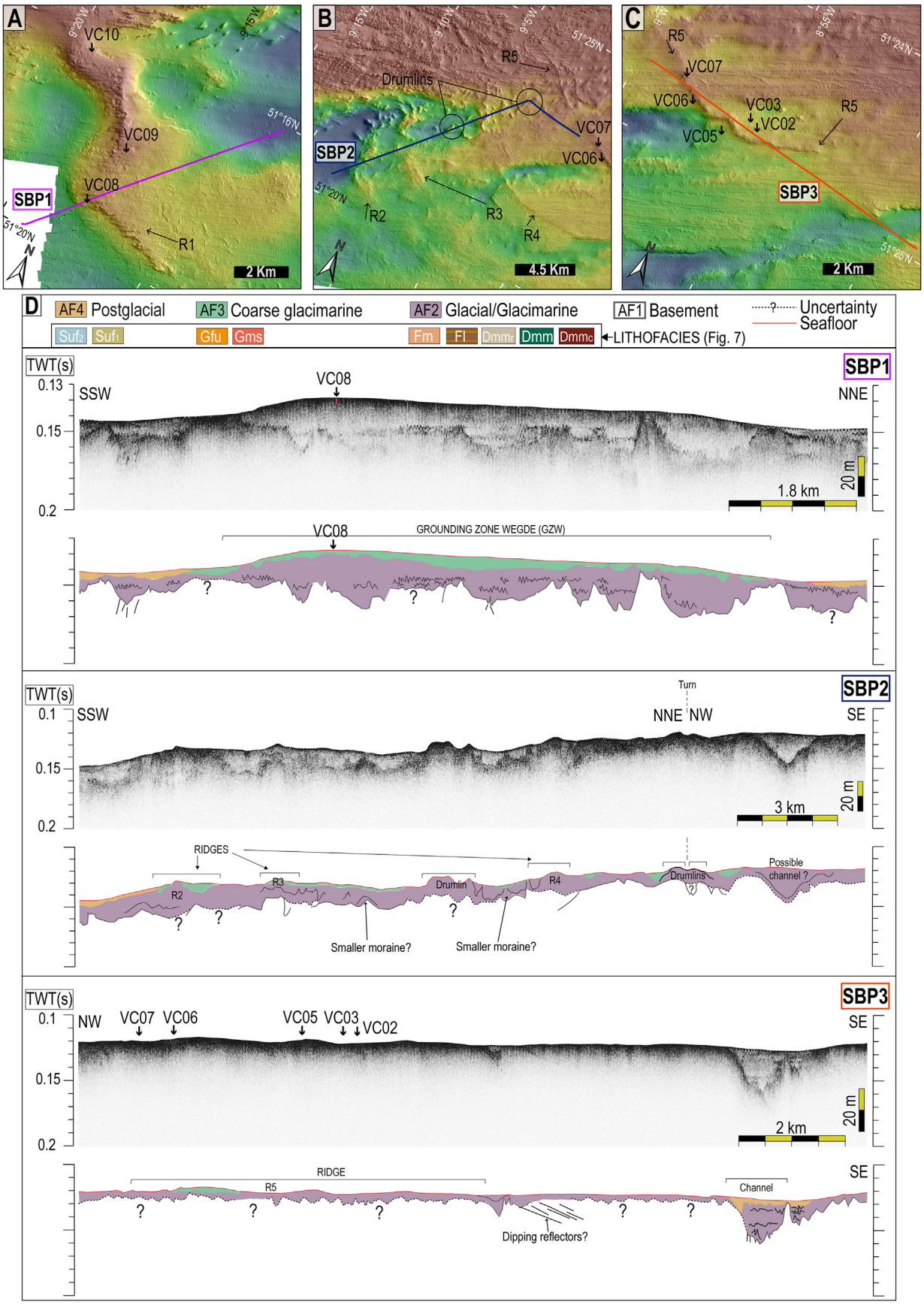

Fig. 5. Uppermost panels A, B and C show the location on the bathymetry of the sub-bottom profiles (SBP1, SBP2 and SBP3) along with sediment core locations. The core numbers refer to the vibro-cores (VC) from research cruise CE1601 and are reported in Table 1. D) Each seismic line is presented in the original (upper panel) and interpreted (lower panel)

Upper contact is sharp but often disturbed as the result of the core recovery process. This facies is mostly found in the core catchers and therefore the lower contact is unknown. Fossil content consists mostly of broken valve shells, typically highly abraded but occasionally in good condition especially in coresVC05 and VC06. Small gastropods and occasional benthic foraminifera are also found within this facies. *Elphidium* spp (e.g. *E. crispum*) and *Ammonia falsobeccarii* are found in cores VC05 (40–67% and 20–90% of the total benthic foraminiferal fauna, respectively) and VC03 (~35% of the total for both species). For the latter core, minor percentages of *Quinqueloculina lata* (abundances ~20%) and *Cibicides lobatulus* (abundances ~15%) are also found (Figs. 7 and 8). One AMS radiocarbon date on shell fragments from facies Dmm_c in core CE1601-VC05 dated 41,082 ± 772 cal yr BP (SUERC-97285; Fig. 7, Table 2).

Lithofacies Dmm is a thin bed (~40 cm) of friable, massive diamicton, only found in one core (105-64 cm in VC06; Fig. 7). It is dark greyish brown (2.5Y 4/2), clast-supported massive diamicton containing abundant gravel-to pebble-sized clasts in a sandy-mud matrix and with no evidence of primary sedimentary structures. The upper contact is irregular while the lower contact corresponding with the core catcher appears sharp and disturbed. No shear strength measurements were obtained in this facies due to the lack of cohesion. Biogenic content consists mostly of shell fragments. One AMS radiocarbon date on valve shells from facies Dmm in core CE1601-VC06 dated 9609 ± 174 cal yr BP (SUERC-97286; Fig. 7, Table 2).

Lithofacies Dmm_r is found in two cores (51-39 cm in VC03 and 76-62 cm in VC05; Fig. 7). It has a dark grey to dark greyish brown colour (2.5Y 4/2) and consists of matrix-supported diamicton containing fewer pebble-to gravel-sized clasts compared to lithofacies Dmm. The clasts deform silt/clay stringers, showing evidence of ductile deformation of the material. The clasts are especially visible in the X-radiographs in the muddy-silt matrix (Fig. 6). There are erosive upper and lower contacts (unconformities) in VC03 and VC05 (Fig. 7). The biogenic content is low and mainly consists of gastropods and rare foraminifera including *Anomalina flintii*, *Bulimina fusiformis*, *Quinqueloculina lata*, *Quinqueluculina seminula* and *Rosalina anomala* (Fig. 8). Two radiocarbon dates were obtained from Dmm_s. In VC05, a bivalve shell sampled from the middle part of this facies yields an age of 9582 ± 165 cal yr BP, and in VC03, a gastropod sample from the top of the facies resulted in an age of 9241 ± 488 cal yr BP (Fig. 7, Table 2).

Lithofacies Fm is found at the bottom of two cores (22-3 cm in VC02 and 214-203 cm in VC08; R1 and R5, respectively; Fig. 7). It consists of dark greyish brown (2.5Y 4/3), moderately stiff (20–38 kPa), silty massive mud. This facies is found at the bottom core and therefore the lower contact is unknown. The coarser sediment at the bottom of core VC02, however, is not considered to be *in situ* (question mark in Fig. 7) likely due to loosen material from the core top following sampling method. The upper contact is irregular-sharp. The homogeneous texture of facies Fm is confirmed by the X-ray images where no traces of bioturbation, lamination and gravel-sized clasts have been observed (Fig. 6). Biogenic material is rare and is dominated by minute specimens of the benthic foraminifera *Elphidium clavatum* (40–60% of the total count) with a smaller contribution (abundances ≤10% each) of *Ammonia falsobeccari*, *Anomalina flintii*, *Bolivina inflata*, *Bulimina fusiformis* and *Cassidulina obtuse* (Fig. 8). No dates have been obtained to age-constrain this facies because the limited amount of fossil material available was not sufficient for radiocarbon dating.

Lithofacies Fl is found in two cores (224-51 cm in VC03, 141-76 cm in VC05; R5; Fig. 7). It ranges in thickness between 1 and 2 m, consisting of a relatively stiff mud (30–45 kPa), dark greyish brown mud (2.5Y 4/2) with greyish brown to dark grey sandy silt laminae (2.5Y 6/2). Upper and lower contacts for this lithofacies are normally abrupt (Figs. 6 and 7). Lamination is typically horizontal or sub-horizontal and undeformed, apart from the down-warping at the core edges that is attributed to the coring process (i.e. pull-up; lower 1 m of core VC03). The lamination appears rhythmic and the laminae form couplets with a sharp-based, coarser lower lamina grading upwards into the finer lamina (Figs. 6 and 7). This repetition of bands can also be detected on the X-radiographs showing alternating light and dark bands, representing respectively coarser (denser) and finer (less dens) sediments (Fig. 6). Rare, small and isolated pebbles and granules can be found within the laminae (e.g. ~120 cm in core CE1601-VC05; Fig. 7). Additionally, laminations observed in cores VC03 and VC05 tend to have a less distinct layering towards the top facies. Bioturbation is not observed. Fossil content is low and with minute foraminifera species (Fig. 8) and rare shell fragments. The species *Elphidium clavatum* dominates in the laminated mud facies in core VC03 ranging between 20% and 90% of the total benthic foraminiferal fauna; whilst it is rare in core VC05 (abundances up to 5%) with a marked increase between 90 and 80 cm (up to 67% of occurrence; Fig. 8). *Bulimina marginata*, *Melonis barleeanus*, *Nonionella labradorica* and *Cibicides lobatulus* occur within the laminated mud in core VC03, all of them not exceeding 10% of the total benthic foraminiferal fauna and decreasing towards the top facies. *Anomalina flintii*, *Bulimina fusiformis*, *Quinqueloculina lata*, *Quinqueluculina seminula* and *Rosalina anomala* occur in both VC03 (especially towards the bottom facies) and VC05. Two radiocarbon dates give an age of 7789 ± 145 cal yr BP for a shell fragment dated at the top of the lithofacies in VC03 and an age of 12,381 ± 245 cal yr BP for a sample of mixed benthic foraminifera towards the top of the facies in VC05 (Table 2).

Lithofacies Gfu consists of a moderately sorted, clast supported gravel and is found in four cores (216-80 cm in VC07, 138-100 cm in VC08, 290-42 cm in VC09, and 480-22 cm in VC10; Fig. 7). Clast size ranges between pebble and cobble size of various lithologies (magmatic-sedimentary), sub-rounded in shape. For three cores, the lower contact is unknow given that the facies is found at the core bottom, except for VC08 where the lower contact is irregular-sharp. The facies occasionally displays a fining-upward trend and a relative increase in biogenic content, mainly bivalves (*Spisula elliptica*), tube worms (*Ditrupa arietina*) and shell fragments towards the top facies.

Lithofacies Gms is a matrix-supported, moderately sorted gravel in a sandy matrix found only in one core (224-138 cm in VC08; Fig. 7). Clasts are sub-rounded in shape; they vary from a magmatic to sedimentary genesis and display a fining-upward trend up to the gradational upper contact; whilst the lower contact is irregular-sharp.

Lithofacies Suf_1 is found in most of the cores (top 3 cm in VC02, 39-9 cm in VC03, 62-20 cm in VC05, 64-5 cm in VC06, 100-6 cm VC08 and 42-20 cm VC09) except for VC07 and VC10 where it is absent (Fig. 7). It consists of olive grey (5Y 4/2), moderately sorted, medium to fine shelly sand, displaying a fining-upward trend in a few of the cores. Abundant bivalve shells (e.g. *Parvicardium ovale*), gastropods (e.g. *Rissoa parva, Turritella communis*) and tube worm fragments (*Ditrupa arietina)* are present together with *Hyalinea*

form. In the legend, each acoustic facies is reported along with the corresponding lithofacies described and interpreted from the cores CE1601. Question marks and dotted lines denote uncertainty. In SBP3, sediment cores are plotted along the seismic line to show their approximate locations. For overview map of the lines refer to Fig. 2A. TWT = Two-Way travel Time.

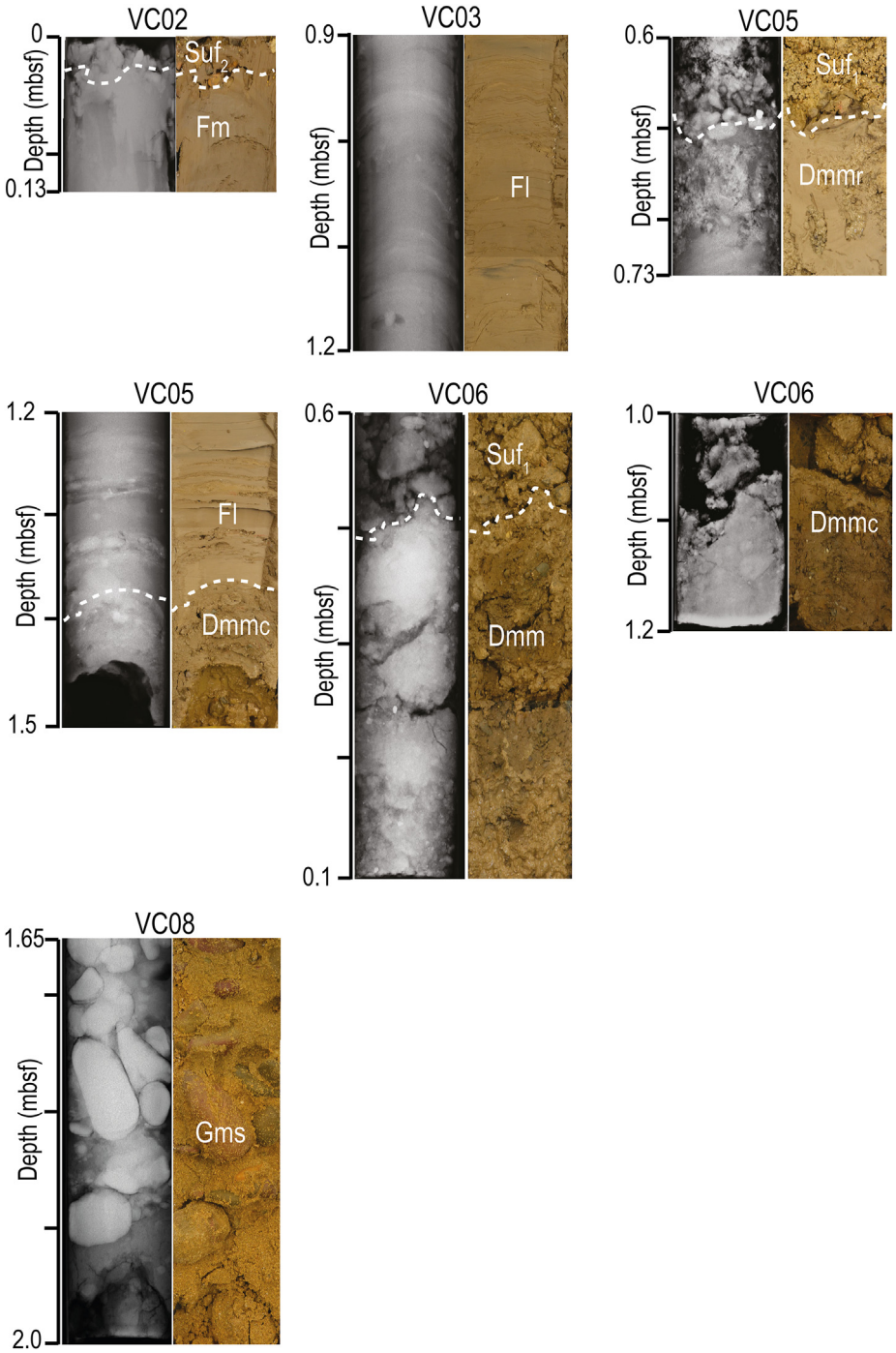

Fig. 6. Representative photographs and X-radiographs of the interpreted lithofacies. Sediment cores including clast-supported gravel were not X-rayed. Dmm_c – compact, massive, matrix-supported diamicton; Dmm – friable, massive diamicton; Dmm_s – matrix-supported diamicton with evidence of resedimentation; Gms – massive, matrix-supported gravel; Suf –fining-upward shelly sand; Fl – laminated mud; Fm – massive mud. The purple dotted lines represent the contact between different lithofacies. For a detailed lithofacies explanation refer to section 4.3 and/or lithofacies summary in Table 4. (For interpretation of the references to colour in this figure legend, the reader is referred to the Web version of this article.)

baltica and *Textularia* spp. (Fig. 8). The lower contact ranges from sharp to gradational. Upper contact is gradational (Fig. 7). Primary sedimentary structures are absent.

Lithofacies Suf$_2$ is found at the top of all the cores, except for VC02 where it is absent. It is between 3 and 20 cm think and it occurs as well-sorted medium to coarse sand with gradational contacts to the underlying lithofacies Suf_1. Biogenic material is abundant and similar to Suf_1. Together, Suf_1 and Suf_2 form the uppermost lithofacies that cap the stratigraphic sequences across all cores.

4.6.1. Facies interpretation and depositional processes

The interpretation of the lithofacies follows the same order as the above descriptions and it is combined with the palaeoenvironmental information retrieved from foraminifera analysis.

Facies Dmm_c is the lowermost stratigraphic unit of three cores

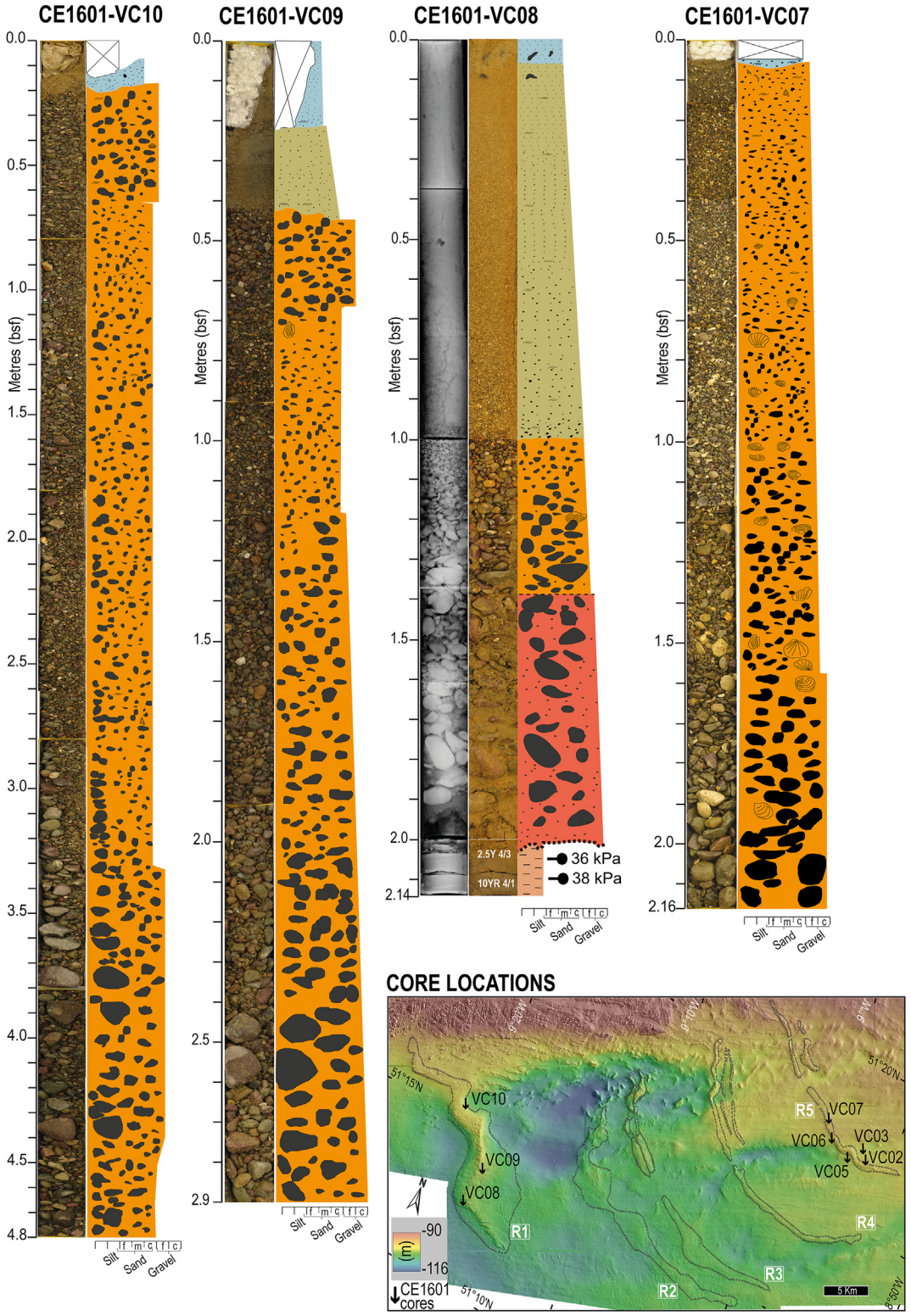

Fig. 7. Core logs for the sediment cores collected at R1 and R5. A map of the core locations on the bathymetry is provided. The lithofacies interpretations are colour coded and coupled with X-radiographs (see Fig. 6 for details). The samples and corresponding calibrated radiocarbon dates (cal yr BP) and shear strength values (kPa) are indicated at the side of the core-logs. The inset at the bottom of core VC05 shows the erratics from the compact diamicton Dmm_c. For facies description and interpretation refer to sections 4.3 and 4.3.1. Lithofacies summary in Table 4. (For interpretation of the references to colour in this figure legend, the reader is referred to the Web version of this article.)

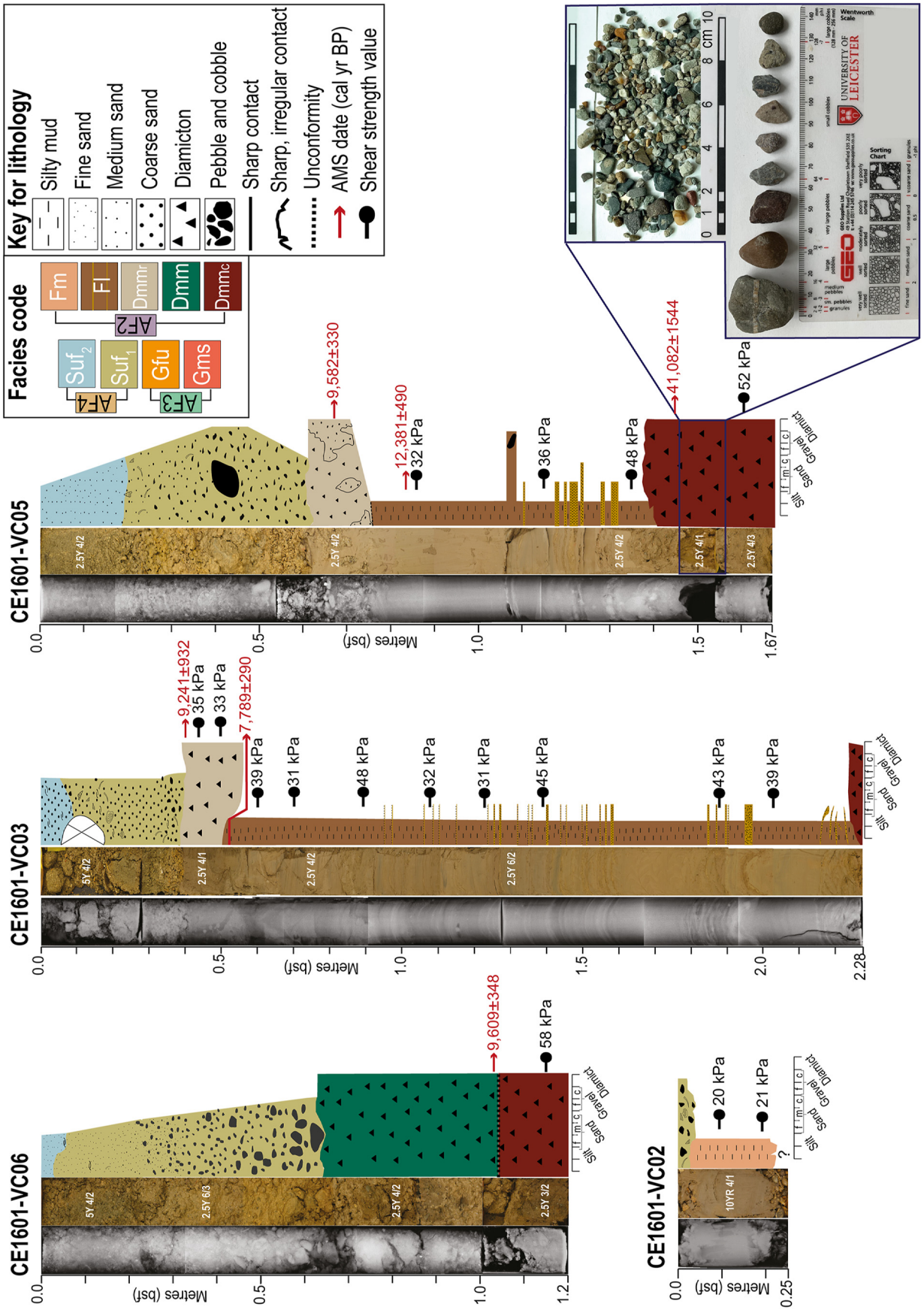

Fig. 7. (*continued*).

Table 4
Summary of the lithofacies description and interpretation associated with the acoustic facies (see Table 3). [1] Smith et al. (2007); [2] Hillenbrand et al. (2005); [3] Ó Cofaigh et al. (2005); [4] Peters et al. (2016); [5] Eyles et al. (1983); [6] Ó Cofaigh and Dowdeswell (2001); [7] Dowdeswell et al. (2015); [8] Lønne (1995) [9] Amorosi et al. (1999); [10] Viana et al. (1998).

Acoustic Facies	Lithofacies Code	Facies position in core	Description	Interpretation
AF2	Dmm_c Compact, massive diamicton	VC03 – 228-224 cm in VC05 VC05 – 167-141 cm VC06 – 120-105 cm	Massive, matrix-supported, compact (~60 kPa) diamicton, 10-30 cm thick. Sharp upper and unknown lower contact. Fossil content: valve shells (chipped but unabraded) and benthic foraminifera.	Sub-glacial till with incorporated reworked and compressed existing marine sediment [1], [2], [3], [4].
	Dmm Friable diamicton	VC06 – 105-64 cm	Friable/massive diamicton in a sandy-mud matrix, ~75 cm thick. Sharp lower and upper contact. Increase in biogenic content upward (mainly shell fragments).	Debris flow [5].
	Dmm_r Matrix-supported diamicton	VC03 – 51-39 cm VC05 – 76-62 cm	Max 20 cm thick. Matrix-supported diamicton with deformed silt/clay stringers. Irregular-sharp lower contact. Erosive upper contact. Biogenic content (gastropod and rare foraminifera).	
	Fl Laminated silty mud	VC03 – 224-51 cm VC05 – 141-76 cm	Stiff (30-45 kPa) mud beds >1 m interbedded with sandy silt laminae. Sharp contacts between muddy-sand couplets of parallel to sub-parallel geometry. Rare pebbles and granules within the laminae. Bioturbation absent. Fossil content is low and dominated by foraminifera *Elphidium clavatum*.	Settling from seasonal meltwater plumes in an ice-proximal to distal environment. High turbidity with possible shorefast sea ice formation [6], [7].
	Fm Massive, homogeneous silty mud	VC02 – 22-3 cm VC08 – 214-203 cm	Moderately stiff (20-38 kPa) mud beds max 25 cm thick. Unknown lower contact. Sharp-irregular upper contact. Low biogenic material dominated by benthic foraminifera (*Elphidium clavatum*).	
AF3	Gms Massive, matrix-supported gravel	VC08 – 224-138 cm	Moderately- sorted gravel in sandy matrix, around 125 cm thick. Irregular-sharp lower contact. Sub- rounded clasts in a fining upward trend towards a gradational upper contact.	Ice-proximal glacimarine deposit [8].
	Gfu Upward- fining gravel	VC07 – 216-80 cm VC08 – 138-100 cm VC09 – 290-42 cm VC10 – 480-22 cm	Moderately- sorted, sub-rounded pebbles. Max 450 cm thick. Fining-upward trend coupled with increase in fossil content (bivalve and tube worms).	
AF4	Suf_1 Shelly, fining-upward sand	VC02 – 0-3 cm VC03 –39-9 cm VC05 – 62-20 cm VC06 – 64-5 cm VC08 – 100-6 cm VC09 – 42-20 cm	Uppermost unit for all the cores, max 125 cm thick. Medium to fine sand fining upward. Abundant biogenic material (bivalve shells, gastropods, tube worm). Sharp to gradational lower contact. Gradational upper contact.	Shelf bottom current winnowing. Modern sedimentation [3], [9], [10].
	Suf_2 Well-sorted, shelly sand	Top cores (between 3 to 20 cm), except for VC02.	Uppermost unit for all the cores, max 30 cm thick. Well-sorted medium to coarse sand. Biogenic material similar to Suf_1. Gradational lower contact.	

and it is interpreted as a subglacial till. The relatively high shear strength measurements, a massive structure with disperse clasts in silt-matrix are consistent with loading and vertical compaction by an overriding glacier and indicate deposition as subglacial till (e.g. Evans et al., 2006; Ó Cofaigh et al., 2007). This facies is the lowermost stratigraphic unit of three cores located near R5 (Fig. 7) and it is the dominant facies of the morainic ridges and till sheets identified as AF2 (Fig. 5). The fragmented biogenic material and temperate microfossils (e.g. *Ammonia falsobeccari*, *Quinqueloculina lata*) in the diamicton suggests the incorporation of older marine sediments over which an ice sheet advanced (Ó Cofaigh and Evans, 2001a; García et al., 2011; Hillenbrand et al., 2013; Peters et al., 2016). A number of chipped but not abraded valve shells collected at the bottom of VC05 dated to 41,082 ± 772 cal yr BP indicating that the sediments at the sites were reworked; thus, the date provides a maximum/relative age for a grounded ice sheet advance over the core sites. The clast rich and consolidated character of Dmm_c also resembles the Melville Till in the central Celtic Sea. The Melville Till is considered the marine equivalent of the Irish Sea Till that outcrops along the south coast of Ireland (Ó Cofaigh and Evans, 2007; Ó Cofaigh et al., 2012a, 2012b; Scourse et al., 1990, 2019). The presence of Dmm_c on this part of the shelf is therefore the closest occurrence to the coastline of the Melville Till.

The variation in clast shape, size and lithology, the absence of internal sediment structures and the presence of mostly fragmented shells suggest a similar depositional process for both facies Dmm (VC06) and Dmm_r (VC03, VC05). They are interpreted as subaqueous debris flows from the oversteepened side of R5 (Fig. 7; Eyles et al., 1983; Hillenbrand et al., 2005). Similar radiocarbon ages ranging from 9609 ± 174 cal yr BP (Dmm) to 9582 ± 165 cal yr BP and 9241 ± 488 cal yr BP (Dmm_r) are also derived from the two facies. These dates further suggest that the downslope remobilisation along R5 occurred at around the same time but resulted in slightly different facies. Similar environments have been found in the eastern Ross Sea, Antarctica, where the palaeo-grounding line is coupled with debris flows deposited on the topset and foreset (seaward) of the ridges (Prothro et al., 2018; Majewski et al., 2020). High sediment supply in an ice marginal to proximal depositional environment can further produce instability of the ridge sides resulting in mass-flow deposits (Ó Cofaigh and Dowdeswell, 2001). However, the ages reported for the two facies suggest that the mass flow likely occurred around 9.5 cal ka BP and therefore after the retreat of the ice margin from this location.

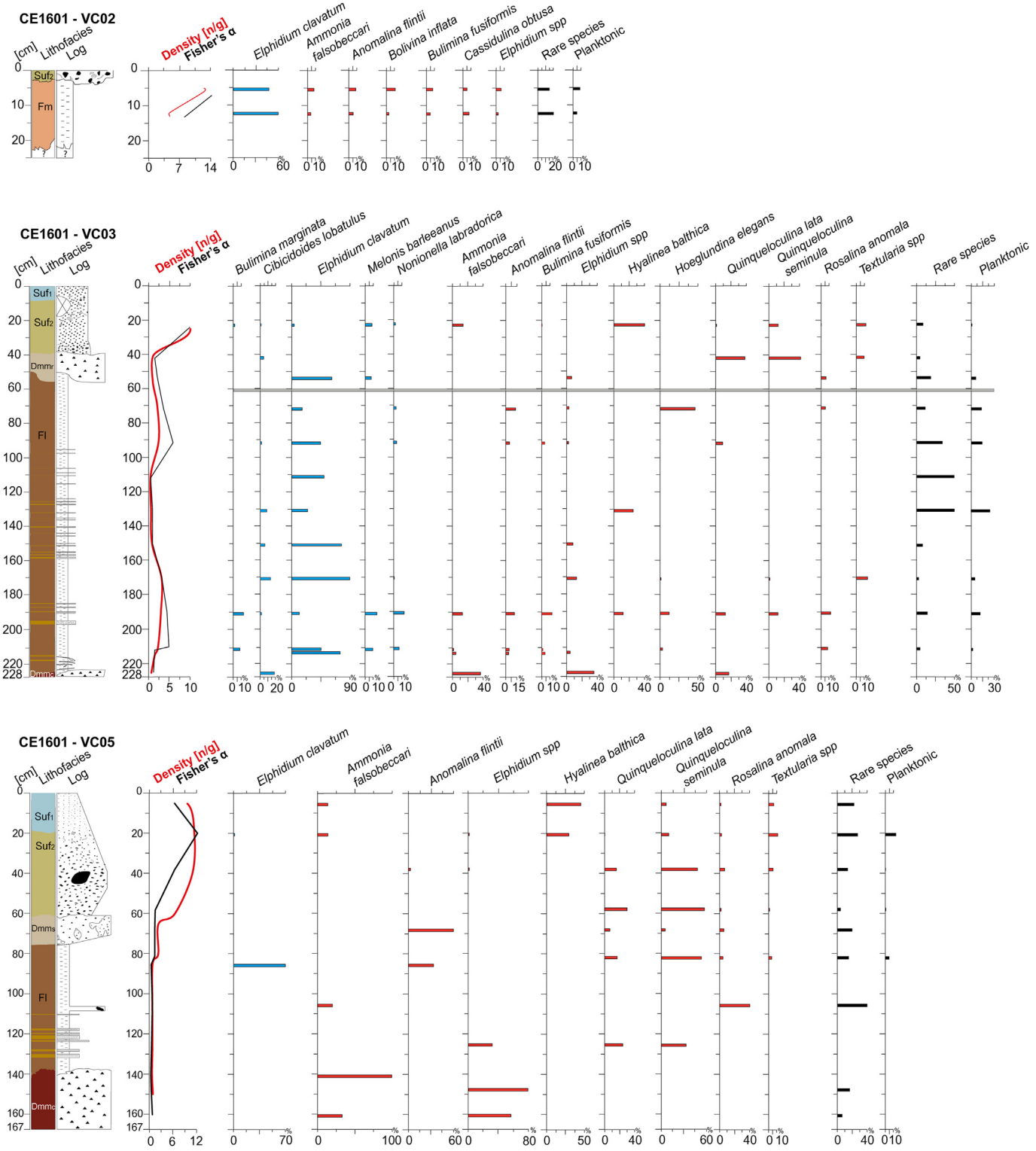

Fig. 8. Micropalaeontology of cores VC02, VC03 and VC05 collected near R5. Only species that comprise 5% or more of the total foraminiferal count in each core are plotted; other species are included in "rare species". Species indicating cold conditions are reported in light blue, whereas more temperate species are indicated in red. Dark grey bar in VC03 represents a barren sample. The density (n/g) and Fisher's α values are shown. (For interpretation of the references to colour in this figure legend, the reader is referred to the Web version of this article.)

The relatively clast-free, rhythmically laminated and relatively stiff mud (30–45 kPa) of lithofacies Fl in cores VC03 and VC05 is interpreted as suspension settling from turbid meltwater, possibly beneath a cover of sea ice thereby explaining the absence of bioturbation and IRD (Ó Cofaigh and Dowdeswell, 2001; Kilfeather et al., 2011).

Based on lithology, moderate shear strength (20–38 kPa) and micropalaeontology, the greyish brown mud of lithofacies Fm in

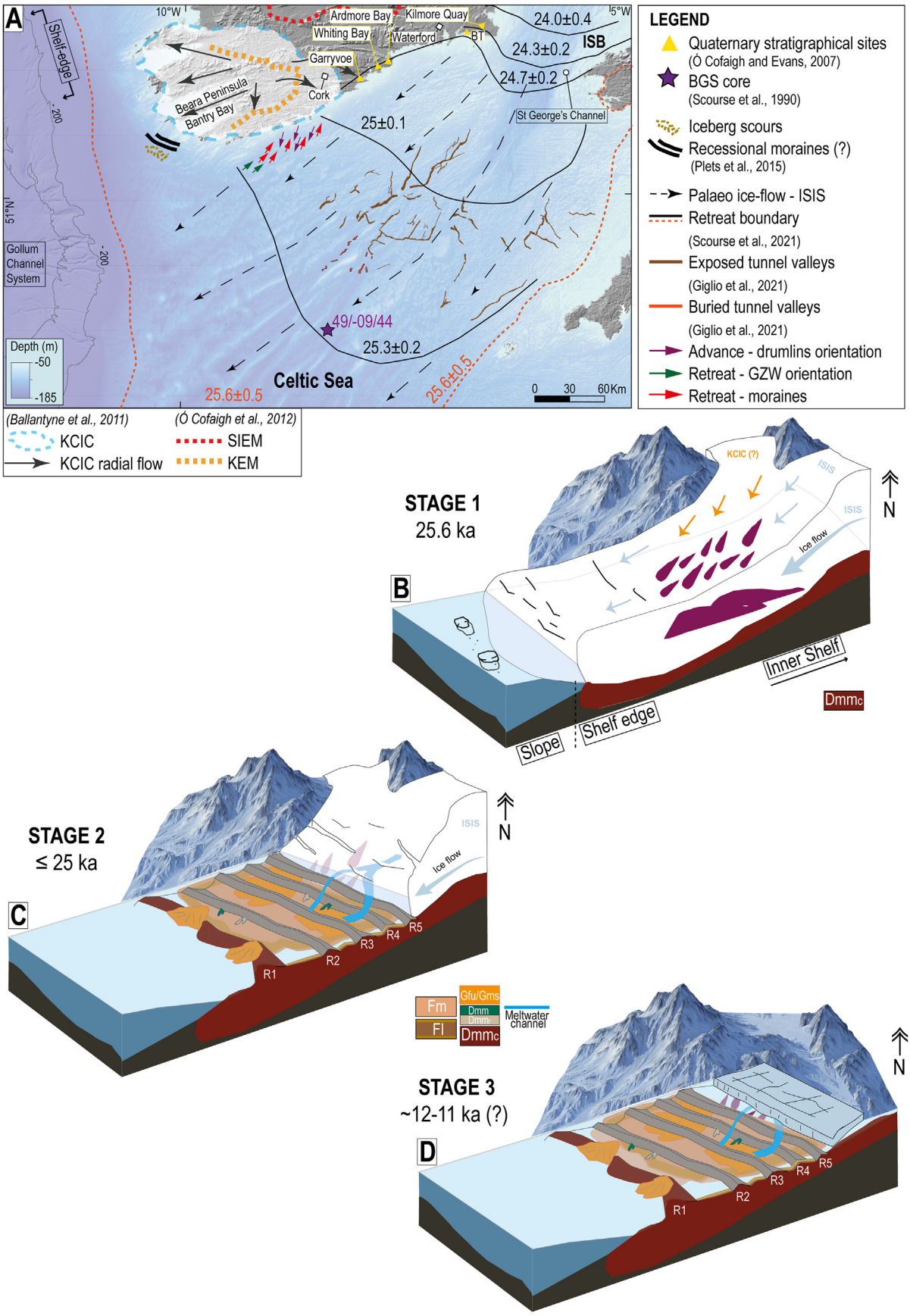

Fig. 9. A) Schematic illustration for the southern BIIS during last glacial period. Dotted arrows indicate the generalised path flows of the Irish Sea Ice Stream (ISIS) towards the shelf edge and crossing the study area offshore south-west Ireland. The orientation of the mapped landforms is indicated along with key geomorphological and stratigraphic locations in

cores VC02 and VC08 is also interpreted as suspension settling from turbid meltwater and it is correlated to the top of facies Fl where the laminations tend to have a less distinct layering. The lack of lamination in the massive mud (Fm) may be associated with an increasingly ice-distal depositional setting or sea-ice formation with the dominance of lithogenic over biogenic detritus (Ó Cofaigh and Dowdeswell, 2001; Hillenbrand et al., 2005). Such an environment may also justify the low diversity, low abundance of foraminifera and/or the presence of small individuals found within both facies Fl and Fm primarily dominated by cold-water species of *Elphidium clavatum* (Fig. 8).

On the other hand, high sedimentation rate during rapid meltwater discharge can also suppress the typical laminae as well as reduce abundances and low species diversity, as presently found in West Antarctica (Alve, 1999; Smith and Andrews, 2000; Ó Cofaigh and Dowdeswell, 2001; Majewski et al., 2020). Two radiocarbon samples from the laminated mud dated 7789 ± 145 cal yr BP (VC03) and 12,381 ± 245 cal yr BP (VC05). Due to the close vicinity to the debris flow of facies Dmm_r, the former is considered unreliable for Fl due to possible sediment reworking (question mark in Table 2). Thus, based on the date in VC05, Fl and Fm can be inferred to have been deposited after ice margin retreat from around 25.3 ka (BRITICE-CHRONO reconstruction) to around 12.4 ka (Fig. 7). Given the potentially low sedimentation rate, it is therefore more likely that the presence of sea ice inhibited fauna colonisation as well as the deposition of the laminae. All the evidence reported above, indicates that facies Fl and Fm have been deposited in glacimarine conditions, potentially recording the transition from ice marginal to distal followed by a sea ice cover continuous to the Younger Dryas Stadial (ca. 12.9–11.5 cal ka BP; Rasmussen et al., 2006).

Although present in VC02, VC03, VC05 and VC08, these laminated and massive mud facies (Fl and Fm) seem to be completely missing from the other cores from R1 as well as from the ones of the westernmost R1. This is possibly a result of erosion, lack of recovery or, in general, the position of the core relative to the ridge. The cores collected on either side of the ridges' crests have a thicker record of Fl (i.e. VC03 and VC05) compared to those on top or along the ridge's slope that do not have this facies. The lack of Fl in core VC06, between facies Dmm_c and Dmm, can be considered as an unconformity caused by the debris flow deposit of Dmm that might have eroded the sediments (Fig. 7).

Lithofacies Gfu is found in cores VC07, VC08, VC09 and VC10 and it is overlain at the top by lithofacies Suf_1 and Suf_2. At the bottom of core VC08 lithofacies Gfu overlays Gms that in turns overlays the massive mud (Fm; Fig. 7). Based on clast abundance and lithologic similarities, Gfu and Gms are interpreted as coarse grained outwash materials deposited in an ice proximal subaqueous setting (McCabe and Eyles, 1988). The biogenic content recognised in the pebbly facies consists of marine fauna implying deposition in a marine setting rather than a terrestrial environment and the relatively low proportion of broken tests also suggests limited reworking. In core VC08, lithofacies Gms is deposited unconformably over the basal massive mud (Fm; ~20 cm thick). A switch in deposition between fine and coarse sediments reflects typical facies variations across an ice-proximal glacimarine environment (Lønne, 1995).

Lithofacies Suf_1 and Suf_2 cap all of the cores and are interpreted to be modern sediment deposits based on lithology, structure (fining upward trend), biogenic abundance and stratigraphic position (e.g. Amorosi et al., 1999; Viana et al., 1998; Peters et al., 2016). Among the more commonly recognised foraminifera species (e.g. *Quinqueloculina seminula*, *Ammonia falsobeccarii*) in the Suf facies association, Textularia sp, *Hyalinea bathica* and *Quinqueloculina lata* were also found. The suborder *Textulariina* has been described as a dominant taxon present in recent/modern sediments and common in coarser sediments (Murray, 1979). In post glacial sediments, foraminiferal density is found to be the highest, indicating increased surface water productivity coupled with a weakening of bottom current energy (fining upward trend; Fig. 7; Peters et al., 2020). Hence, the foraminifera analysis shows significant differences in species composition with the almost complete disappearance or drastic decrease in *E. clavatum*, which is an indicator for a glacimarine environment (Fig. 8; Hald et al., 1994; Hald and Korsun, 1997). Sediments with similar lithology and foraminiferal content have been sampled in the Celtic Sea and Celtic Deep and also interpreted as modern day sedimentation (Pantin and Evans, 1984; Furze et al., 2014).

Lithofacies, therefore, range from Late Pleistocene subglacial to glacimarine sediments to Early Holocene sands at the core tops (Table 4). The micropalaeontology shows that the species density is the highest at the core tops (5–10 n/g) and drops with increasing depths (0.1–2 n/g), for example at the laminated mud (Fl) and compact diamicton (Dmm_c) (Fig. 8). A similar trend is shown by the Fisher's α index where the species diversity declines with increasing core depths. The planktonic foraminifera abundances range between 4 and 8% in all the cores and up to 25% in VC03 (Figs. 7 and 8).

5. Discussion

5.1. Local reconstruction of the glacial history offshore SW Ireland

The link between the new geomorphological and stratigraphical data presented in this study allow to refine the reconstruction of the BIIS last glacial advance and retreat and of palaeoenvironments offshore southwestern Ireland. The orientation of newly mapped relict glacial features, such as drumlins, a GZW and moraines, suggest ice flowing firstly sub-parallel and later parallel to the present-day coastline (Figs. 2B and 9A), thus suggesting a shift in the pattern of ice flow through space and time. For the first time, the presence of subglacial till provides direct indication of grounded ice ca. 30 km offshore southwestern Ireland. Laminated and massive muds overlying the diamict indicate ice retreat from the core sites and sedimentary deposition under glacimarine conditions followed by the establishment of a modern marine environment. The interpretation of these datasets is combined in a three-stage model for the evolution of the study area during the late Quaternary (Fig. 9).

5.1.1. Stage 1: ice advance onto the shelf

A first stage characterised by ice advance onto the shelf offshore

the south coast of Ireland (Ó Cofaigh and Evans, 2007; Ballantyne et al., 2011; Ó Cofaigh et al., 2012a, 2012b; Plets et al., 2015). The chronology of the major retreat limits is plotted over the bathymetric map of the Celtic Sea shelf and refers to the isochrones reconstructed by Scourse et al. (2021). The reconstructed evolution of the study area during the LGM can be summarised as: B) Stage 1: the ISIS reached the shelf edge ~25.6 ka BP. At this time the drumlins were formed. The two possible sources of ice flowing and depositing the drumlins are the KCIC (orange arrows) and the ISIS (light blue arrows). See text for details. Deposition of compact diamicton (Dmm_c) is ongoing. C) Stage 2: ice retreats northeastward and is punctuated by several still-stands recorded by the GZW (R1) and retreat moraines (R2-R5 and eastward ridges) overprinting the drumlins. Ice marginal to distal glaciomarine settings are established and possibly continued until stage 3. However, timing of events between stages 2 and 3 is uncertain. D) Stage 3: cool conditions in a low energy environment with potential sea-ice cover. This stage is possibly continuous during deglaciation until the Younger Dryas Stadial. Figures are not to scale. The spatial extent of the lithofacies and the sea level position are only illustrative. The 'snowy mountain' 3D model used in the illustrations was retrieved from the opensource ArtStation platform (https://www.artstation.com/artwork/AKdrX). (For interpretation of the references to colour in this figure legend, the reader is referred to the Web version of this article.)

south-west Ireland (Stage 1; Fig. 9B) is marked by the drumlins imaged through the bathymetric and sub-bottom data (Figs. 3 and 5). Drumlins have long been considered indicators of former ice directions and they have been used in many formerly glaciated areas to model the dynamics of Quaternary ice sheets (Menzies, 1979; Clark et al., 2009a, 2009b; Livingstone et al., 2010, 2012; Iverson et al., 2017). Given the relatively close location of the study area to the coastline and the SSW long-axis orientation of the drumlins, there are different possible sources of ice that could have contributed to their formation.

The first is linked to a possible offshore extension of the KCIC during the last ice advance (Stage 1; Fig. 9B). The location of the field of drumlins implies grounded ice more than 25 km south of the present-day coastline (Fig. 9A). The locally-nourished KCIC has been reconstructed to radiate outwards from an ice divide near the head of the Kenmare River, north of the Beara Peninsula (Fig. 9A) (Farrington, 1936; McCabe, 1987; Warren, 1991; Ballantyne et al., 2011). While to date evidence for the offshore extension of the ice cap is very limited, iceberg ploughmarks were mapped ~30 km offshore Bantry Bay, and tentatively linked to the retreat and calving of the last KCIC (Fig. 9A) (Plets et al., 2015). Therefore, an offshore KCIC extension to the south of County Cork would have been possible. However, qualitative analysis on the lithics within Dmm_c (base of cores VC03, VC05, VC06) does not point towards inland petrologies. Inland tills, for example the Blackhall Till cropping out in Waterford coastal sections (BT in Fig. 9A), are characterised by granitic lithologies (van der Meer et al., 1994; Gallagher and Thorp, 1997; Gallagher et al., 2004). The Dmm_c lithics display instead various lithologies, including magmatic, metamorphic and sedimentary clasts (inset in Fig. 7). The 'exotic' erratic assemblages and shell fragments found in the compact diamicton seem to exclude a full inland origin.

Alternatively, the direction of the drumlins could indicate a possible formation under the ISIS last ice advance across and subparallel to the coastline and towards the shelf-edge (Fig. 9A and B). This hypothesis appears consistent with what is known about the ISIS, as it impinged across the present southern Irish coastline during the last ice advance. The inland incursion of ice is thought to have occurred across a narrow zone of $\leq$1–3 km, based on IST deposits cropping out intermittently along the coast (Ó Cofaigh et al., 2012a, 2012b). Therefore, the formation of the drumlins under the ice streaming across the southern coastline and towards the southwest once it reached County Cork seems spatially feasible. Based on the sub-bottom data discussed in sect. 4.2, the glacial/glacimarine AF2 blankets the acoustic basement across the entire study area. Therefore, it is also possible that the area was at the confluence of the ISIS and the KCIC and the sediments and drumlins deposited at this stage are evidence of such confluence. This reflects previously outlined scenarios of ice advance, where the BIIS is a combined ice sheet comprised of satellite domes and ice streaming offshore (Clark et al., 2012).

The one AMS date on shell fragments from the till blanketing the study area yielded an age of 41 ± 7.7 cal ka BP (CE1601-VC05; Figs. 5 and 7, Table 2). This old date is due to the 'reworked' nature of till samples (Ó Cofaigh and Evans, 2007; Ballantyne and Ó Cofaigh, 2017; Callard et al., 2018; Ó Cofaigh et al., 2019). This is also the case for the wide range of dates from >50,000 to 20,000 years BP obtained on shell fragments from the Irish Sea Till at different locations in southern Ireland (from Garryvoe to Kilmore Quay; Fig. 9A). The age of the till in the study area therefore correlates with that of the IST onshore (Ó Cofaigh and Evans, 2007; Ó Cofaigh et al., 2012a, 2012b) and to its offshore counterpart the Melville Till (Evans and Ó Cofaigh, 2003), which suggests it was deposited sometime prior to ~25 cal ka BP (Praeg et al., 2015; Scourse et al., 1990, 2021). This till provides further evidence of a grounded BIIS advance across the south-west of Ireland.

5.1.2. Stage 2: ice retreat from and across the shelf

The second stage is characterised by ice retreating across the shelf (Stage 2; Fig. 9C). The orientation of the GZW and sequence of moraines denotes ISIS withdrawal towards the Irish coastline (green and red arrows; Fig. 9A).

Although previous reconstructions report a short-lived persistence of the ISIS onto the Celtic Sea shelf (Scourse et al., 1990, 2021; Scourse and Furze, 2001), the new data presented in this study clearly show that ice retreat was interrupted by prolonged still-stands that took place after ~25 ka. R1 was deposited as a GZW and it is now preserved as a large ridge on the seafloor (Fig. 9C). The position of the GZW or R1 is here interpreted as a distinct ice margin during overall retreat towards the inner shelf offshore Cork. The series of submarine moraines, eastward of the GZW, are also associated to the ISIS retreat phase. Each individual ridge records changes in the position of the ice margin during withdrawal accounting for repeated still-stands across this portion of the shelf (e.g. Dowdeswell et al., 2008; Ó Cofaigh et al., 2008, Ò Cofaigh et al., 2012a, 2012b). Furthermore, the moraines are cross-cut along their lengths by meltwater channels (Figs. 2A, 4A and 9C). This indicates drainage evolution during deglaciation as the channels continued to drain water as the ice sheet retreated across the area (Livingstone and Clark, 2016; Giglio et al., 2021).

The formation of grounding line systems seems to be promoted by pre-existing local highs in the seafloor topography (Lønne, 1995). Given the extent of exposed bedrock in the area, it seems likely that the acoustic basement might have acted as pinning point for the ice margin during retreat (SBP1 in Fig. 5A, D). The relatively good preservation on the seafloor of the GZW together with the sequence of moraines to the east suggests that these landforms are related to the final stages of ice streaming in the area (e.g. Dowdeswell et al., 2016, 2020).

The thinning of the sedimentary units to the east, as detected in the seismic data (AF2, AF3; Fig. 5D), suggests a progressive decrease in sediment flux to the grounding zone (Dowdeswell and Fugelli, 2012; Batchelor and Dowdeswell, 2015). It seems feasible that during the initial phase of ice-margin retreat after ~25 ka, sediment and glacial meltwater were more abundant resulting in the build-up of the western and larger R1/GZW (Figs. 4B and 9C – Stage 2). Furthermore, the GZW is draped by coarse glacimarine sediments (i.e. fan-like) imaged in the seismic data (AF3) and ground-truthed in four cores (Gms, Gfu; Fig. 7). Such a sedimentation unit requires a quasi-stable ice terminus for some time in order to accumulate and aggrade (Powell and Alley, 1997). This implies stability of the grounding line at R1 for a significant amount of time. Conversely, in the later stage of ice withdrawal, a lower sediment supply resulted in smaller ridges (Fig. 9C), thus suggesting lower accumulation rates at the grounding line and greater ice evacuation from the shelf (Powell, 1990). Although in our case the timing of formation of the ridges is not available, their sequential pattern implies that the ISIS underwent major readjustments during deglaciation.

During the north-eastward retreat of the ice margin after ~25 ka, laminated and massive muds (Fl and Fm) were deposited as part of the glacial/glacimarine unit visible in the sub-bottom data (Figs. 5 and 9C, Table 3). Their character indicates settling from a buoyant meltwater plume of a retreating tidewater glacier (Ó Cofaigh and Dowdeswell, 2001). The foraminifera analysis on glacimarine muds indicated minor proportions of more temperate water species, such as *Quinqueloculina* spp, *Rosalina anomala*, *Anomalina flintii* and *Textularia* spp. Their presence tends to increase towards the top of the facies (Fig. 8). Previous studies on foraminiferal assemblages along the western Irish shelf did not notice the co-occurrence of temperate with cold water species, but actually the

opposite (e.g. Callard et al., 2018; Peters et al., 2020). However, temperate waters species have been found together with Elphidium crispum (cold water species; Murray, 1979) in samples from this area. This mixing of cold and warm water species has been documented in the glacimarine sequences elsewhere in the Celtic Sea shelf and described as a typical characteristic of the Melville Laminated Clay deposited after 25 ka BP (Austin and McCarroll, 1992; Furze et al., 2014; Praeg et al., 2015; Scourse et al., 1990, 2002, 2019). Therefore, the laminated mud in our cores VC03 and VC05 can be correlated to the Melville Laminated Clay and consequently to the onset of glacimarine deposition after 25 cal ka BP during northward retreat of the ice margin across the Celtic Sea (Praeg et al., 2015; Scourse et al., 2019).

5.1.3. Stage 3: persistence of cold conditions between 24 ka and the Younger Dryas

The third stage is characterised by the persistence of cold conditions during deglaciation, or at least the combination of cold environments with some temperate character (Stage 3 – Fig. 9D), as shown by chronology and micropalaeontology towards the top of the laminated and massive mud facies (Fl and Fm; Fig. 8).

A mix of benthic foraminifera from glacimarine sediments in core VC05 yielded an age of 12.4 ± 2.5 cal ka BP (Fig. 7, Table 2). This age is considerably younger than expected for glacimarine conditions following the initial deglaciation of the Celtic Sea shelf, which is thought to have been ice free after 20 ka BP (e.g. Scourse et al., 2021). However, the laminated nature of the sediments, with no obvious erosional or sharp contacts within the facies, together with the date of ~12 cal ka BP seem to suggest continuous deposition between deglaciation and the Younger Dryas (YD: 12.9–11.7 cal ka BP; Rasmussen et al., 2006). Given that there is no evidence of erosional lower contact between the laminated mud and compact diamicton (Dmm_c), the deposition of the laminated mud was potentially initiated earlier, probably following the ice margin retreat around 25.3 ka (Fig. 9A; Scourse et al., 2021).

Scattered evidence from sediment cores offshore Ireland have conveyed deposits with similar age. This includes cores offshore Galway Bay, along the western Irish seaboard, where Wood et al. (2018) reported isolated clasts in fine-grained laminated sediments and suggested a rather extensive pack ice present at around 12.8 ka BP. Further evidence from Donegal Bay reported a suite of dates from foraminifera in glacimarine sediments yielding ages between 12.3 and 12.8 cal ka BP (Weilbach, 2018). Similar ages from foraminifera in laminated stiff clay from cores retrieved in Belfast Lough dated between 13 and 12.3 cal ka BP and interpreted to be deposited under cold conditions during the YD (Plets et al., 2019).

Evidence reported by Isarin (1997) shows that discontinuous permafrost cover existed in Ireland during the coldest part of the YD, probably as far south as 50°N, with palaeo temperature ranging between −8 °C and −1 °C. Hence, a broad cover of pack ice might have generated quiet and low-energy seabed conditions for the deposition of the upper part of the laminated facies before the establishment of modern marine conditions (Figs. 7 and 9D). Such cold temperatures might have favoured sea-ice cover with discharge of turbid meltwater plumes from a glacier terminus (Clark et al., 2017) that, together, could explain the sparse and minute cold foraminifera specimens found within the laminated mud sediment (Figs. 7 and 8) (Scourse et al., 1990; Syvitski, 1991).

Although this is somewhat hard to reconcile with the current models found in the literature, where the marine margin of the BIIS declined by around 18 ka BP (at the latest; e.g. Scourse et al., 2021), the age reported in this study suggests cold conditions between deglaciation and the YD in this part of Ireland. The young age and characteristics of the laminated and massive mud facies is difficult to explain without sea-ice cover. Further validation of this interpretation and its potential correlation with other sparse evidence across the Irish continental shelf could lead to significant progress on the understanding of the period between deglaciation and the YD in Ireland and on the extent and nature of sea ice cover at such low latitudes.

5.2. Implications for the regional BIIS and ISIS reconstruction

The study area is located some 150 km eastward from the shelf-edge. In a similar pathway indicated by the updated palaeo-ice flow directions (black dotted and arrowed lines; Fig. 9A), the ISIS dynamics across the shelf in southern Ireland may have contributed to the evolution of the Gollum Channel System on the slope. Although iceberg tracks have not been detected in this study and, currently, there are no high-resolution data to resolve the portion of the shelf between westernmost Ireland and the shelf-edge, a possible link between the inner and outer shelf during last glacial advance and retreat should not be excluded.

At a regional scale, the sequence of the GZW and moraines, subperpendicular to the present-day coastline (green and red arrows; Fig. 9A), is the direct result of local ice-margin oscillations. The occurrence of still-stands suggests the ISIS was retreating in an episodic rather than continuous fashion or as a single rapid collapse, at least in this sector of the shelf.

The ISIS is thought to have withdrawn rapidly from the shelf-edge at 25.3 ka and to near St George's Channel at 24.7 ka (Fig. 9A), where the ice margin halted before its final retreat into the Irish Sea at a rate between 150 and 300 ma^{-1} (Chiverrell et al., 2018; Small et al., 2018; Scourse et al., 2019, 2021). However, the stepped retreat proposed in this study is not resolved in the time frame between 25.3 and 24.7 ka of net axial ice margin retreat rate by Scourse et al. (2021). Hence, this shows the importance of our analysis, enabled by the newly acquired high-resolution data, that provide evidence for an episodic retreat behaviour of the western ISIS margin, across southern Ireland (Fig. 9A). Furthermore, this pattern of stepped retreat is commonly found across former ice stream areas of the BIIS, such as the Malin Sea shelf, along with other marine-based palaeo-ice streams of the Barents Sea, eastern Canada and West Antarctica (Ottesen et al., 2005; Shaw et al., 2006; Winsborrow et al., 2010; Jakobsson et al., 2016; Newton and Huuse, 2017; Benetti et al., 2021; Bradwell et al., 2021).

The erosion of a suite of tunnel valleys by the retreating ISIS across the central Celtic Sea shelf has been inferred to occur between 25.6 and 24.3 ka (Fig. 9A; Giglio et al., 2021). It appears that while the ice was eroding the subglacial valleys, it was also depositing the ridges along the westward flank. Local variation in the bathymetry, such as the bedrock highs visible on the seafloor and sub-bottom profiles (Fig. 2A, C, D, 5D), might have acted as pinning points during retreat (Favier et al., 2012). This might have slowed down the pace of ice withdrawal in this area and favoured the formation of the GZW and retreat moraines fed by Irish-based ice. Such a pattern of retreat is commonly observed in marine-based palaeo-ice streams and reflects the variability beneath the ice and how it can influence the rate of retreat (Ottesen et al., 2005; Shaw et al., 2006; Winsborrow et al., 2010; Newton and Huuse, 2017; Bradwell et al., 2021). Although the regional chronological reconstruction helped to place different events in time, the absence of any absolute ages on the tunnel valleys makes their correlation with the GZW and moraines a speculative argument.

Ultimately, the stepped retreat of the ice margin across the Celtic Sea has been established between 25.3 and 25 ka (isochrones by Scourse et al., 2021, Fig. 9A). This means that the deposition of the GZW and moraines took place within a few centuries. This is faster than the reconstructed deposition of ridges at grounding lines (600–1500 years) during ice stream retreat across Pine Island

Bay in Antarctica post LGM (Kirshner et al., 2012; Davies et al., 2017). The palaeo-records appear as useful analogues to test the implication of such a rapid mass loss for modern-day settings and their evolution over the next centuries. Equivalent scenarios of fast ice retreat have already been observed across deglaciating marine areas of Antarctica, such as the Larsen continental shelf. Here, a complex of small moraines around 1.5 m height and spaced ~20 m apart recorded the very rapid regional deglaciation of the shelf (>10 km per year) (Dowdeswell et al., 2020). In our study area, the migration of the ice-stream grounding zone over time cannot be fully resolved with our existing data: additional core sampling from each ridge is required. If in the future this would be available together with additional chronological constraints for the timing of formation of the GZW and moraines in the study area, this would enhance knowledge of grounding line retreat rates within episodes of overall fast retreat. Such information would provide a critical long-term constraint for testing and calibrating ice sheet models.

6. Conclusions

This study presents the first geomorphological and sedimentological evidence of ice-sheet presence on the shelf some 30 km off County Cork, southwest Ireland. The geological record preserved at the seafloor and sub-seafloor were investigated using high-resolution bathymetric and sub-bottom data and sediment cores to reconstruct the last glacial dynamics across the inner shelf:

- A field of drumlins was formed during a phase of south-west ice advance onto the shelf, implying grounded ice more than 25 km south of the present-day coastline. Two possible sources of ice have been considered to form the drumlins, including an offshore extension of the KCIC and the ISIS last ice advance. Although the lithics assemblages in the subglacial till Dmm_c seem to exclude a fully inland origin, the seismic data show glacial/glacimarine unit AF2 blanketing the entire study area. This suggests potential confluence of the ISIS and the KCIC with sediments and drumlins deposited at this stage. This is the first time such convergence is observed that far offshore SW Ireland.
- Compact and massive subglacial till was deposited over the area some time after ~41 cal ka BP. This could have happened during the LGM ice advance onto the shelf incorporating and reworking older marine sediments. The till is correlated to the Irish Sea Till (onshore) and Melville Till (offshore) and it is the first time that this unit has been encountered offshore SW Ireland.
- Ice margin retreat is then recorded by a GZW and a series of recessional moraines fed by Irish-based ice. The newly acquired bathymetric data suggest that the ice margin paused or slowed down a few times offshore the southwestern Ireland before its definite withdrawal into the Irish Sea basin. This implies a local stepped retreat behaviour that, based on the published chronology by Scourse et al. (2021), might have occurred between 25.3 and 24 ka.
- During the stage of ice margin retreat, the laminated and massive mud facies record glacimarine conditions and the transition from ice marginal to distal and potential sea ice cover over the site.
- A calibrated radiocarbon date of ~12 cal ka BP from the upper part of the laminated facies together with low abundance of biogenic material indicates permanence of cold conditions with potential sea ice cover during the Younger Dryas. Although scattered evidence of similar young age deposits is found offshore western and eastern Ireland, it is the first time that this has been encountered in a shallow marine environment in southwestern Ireland and it forms an important marker for future seismic and coring work.

Credit authorship contribution statement

Cristiana Giglio: Conceptualization, Methodology, Formal analysis, Investigation, Data curation, Writing – original draft, review & editing, Visualization. Sara Benetti: Conceptualization, Methodology, Investigation, Resources, Writing – review & editing, Supervision, Project administration, Funding acquisition. Ruth Plets: Methodology, Investigation, Writing – review & editing, Supervision. Paul Dunlop: Investigation, Writing – review & editing, Supervision. Colm Ó Cofaigh: Investigation, Writing – review & editing. Fabio Sacchetti: Software, Data curation, Writing – review & editing. Elaine Salomon: Formal analysis, Investigation.

Declaration of competing interest

The authors declare that they have no known competing financial interests or personal relationships that could have appeared to influence the work reported in this paper.

Acknowledgments

This work was carried out as part of C Giglio's PhD project funded by the Department of Education and Learning at Ulster University (Ph.D. studentship 110118). The work was further supported by the NEIF Radiocarbon NRCF010001 (allocation number 2173.0319). We thank Dr Xiaomei Xu at the Keck C cycle AMS Lab, University of

California, for analysing the small radiocarbon samples. High-resolution multibeam echosounder bathymetric and sub-bottom data and sediment cores presented in this study were acquired by the Integrated Mapping for the Sustainable Development of Ireland's Marine Resource (INFOMAR) programme (www.infomar.ie). INFOMAR is a Department of the Environment, Climate and Communications (DECC) funded national Irish seabed mapping programme, jointly managed and delivered by Geological Survey Ireland and Irish Marine Institute. The regional backdrop bathymetry was derived from the EMODnet Bathymetry portal (www.emodnet-bathymetry.eu). We thank the masters, crew and scientists of the R.V. *Celtic Voyager* and R.V. *Celtic Explorer* who contributed to the collection of all the datasets shown in this paper. Dr Vincent Rinterknecht, one anonymous reviewer and the input of the JQSR Editor in chief Professor Claude Hillaire-Marcel are acknowledged for their detailed and constructive comments, which helped to significantly improve the manuscript.

Appendix A. Supplementary data

Supplementary data to this article can be found online at https://doi.org/10.1016/j.quascirev.2022.107655.

References

Alve, E., 1999. Colonization of new habitats by benthic foraminifera: a review. Earth Sci. Rev. 46, 167–185. https://doi.org/10.1016/S0012-8252(99)00016-1.

Amorosi, A., Colalongo, M.L., Pasini, G., Preti, D., 1999. Sedimentary response to Late Quaternary sea-level changes in the Romagna coastal plain (northern Italy). Sedimentology 46, 99–121. https://doi.org/10.1046/j.1365-3091.1999.00205.x.

Austin, W.E.N., McCarroll, D., 1992. Foraminifera from the Irish sea glacigenic deposits at aberdaron, western lleyn, north wales: palaeoenvironmental implications. J. Quat. Sci. 7, 311–317. https://doi.org/10.1002/jqs.3390070406.

Ballantyne, C.K., Ó Cofaigh, C., 2017. The last Irish ice sheet: extent and chronology. In: Coxon, P., McCarron, S., Mitchell, F. (Eds.), Advances in Irish Quaternary Studies. Atlantis Press, Paris, pp. 101–149.

Ballantyne, C.K., McCarroll, D., Stone, J.O., 2011. Periglacial trimlines and the extent of the kerry-cork ice cap, SW Ireland. Quat. Sci. Rev. 30, 3834–3845. https://doi.org/10.1016/j.quascirev.2011.10.006.

Batchelor, C.L., Dowdeswell, J.A., 2015. Ice-sheet grounding-zone wedges (GZWs) on high-latitude continental margins. Mar. Geol. 363, 65–92. https://doi.org/10.1016/j.margeo.2015.02.001.

Benetti, S., Chiverrell, R.C., Ó Cofaigh, C., Burke, M., Medialdea, A., Small, D., Ballantyne, C., Bateman, M.D., Callard, S.L., Wilson, P., Fabel, D., Clark, C.D., Arosio, R., Bradley, S., Dunlop, P., Ely, J.C., Gales, J., Livingstone, S.J., Moreton, S.G., Purcell, C., Saher, M., Schiele, K., Van Landeghem, K., Weilbach, K., 2021. Exploring controls of the early and stepped deglaciation on the western margin of the British Irish Ice Sheet. J. Quat. Sci. 36, 833–870. https://doi.org/10.1002/jqs.3315.

Benetti, S., Dunlop, P., Ó Cofaigh, C., 2010. Glacial and glacially-related features on the continental margin of northwest Ireland mapped from marine geophysical data. J. Maps 6, 14–29. https://doi.org/10.4113/jom.2010.1092.

Benn, D.I., Dawson, A.G., 1987. A devensian glaciomarine sequence in western islay, inner hebrides. Scot. J. Geol. 23, 175–187. https://doi.org/10.1144/sjg23020175.

Benn, D.I., Evans, D.J.A., 2010. Glaciers and Glaciations, Second. ed. Hodder Education, London.

Bennett, M.R., 2003. Ice streams as the arteries of an ice sheet: their mechanics, stability and significance. Earth Sci. Rev. 61, 309–339. https://doi.org/10.1016/S0012-8252(02)00130-7.

Bowen, D., Phillips, F., McCabe, A., Knutz, P., Sykes, G., 2002. New data for the last glacial maximum in great britain and Ireland. Quat. Sci. Rev. 21, 89–101. https://doi.org/10.1016/S0277-3791(01)00102-0.

Bradwell, T., Small, D., Fabel, D., Smedley, R.K., Clark, C.D., Saher, M.H., Callard, S.L., Chiverrell, R.C., Dove, D., Moreton, S.G., Roberts, D.H., Duller, G.A.T., Ó Cofaigh, C., 2019. Ice-stream demise dynamically conditioned by trough shape and bed strength. Sci. Adv. 5, 1–14. https://doi.org/10.1126/sciadv.aau1380.

Bradwell, T., Fabel, D., Clark, C.D., Chiverrell, R.C., Small, D., Smedley, R.K., Saher, M.H., Moreton, S.G., Dove, D., Callard, S.L., Duller, G.A.T., Medialdea, A., Bateman, M.D., Burke, M.J., McDonald, N., Gilgannon, S., Morgan, S., Roberts, D.H., Ó Cofaigh, C., 2021. Pattern, style and timing of British–Irish Ice Sheet advance and retreat over the last 45 000 years: evidence from NW Scotland and the adjacent continental shelf. J. Quat. Sci. 36, 871–933. https://doi.org/10.1002/jqs.3296.

Callard, S.L., Ó Cofaigh, C., Benetti, S., Chiverrell, R.C., Van Landeghem, K.J.J., Saher, M.H., Gales, J.A., Small, D., Clark, C.D., Livingstone, Stephen, J., Fabel, D., Moreton, S.G., 2018. Extent and retreat history of the Barra Fan Ice Stream offshore western Scotland and northern Ireland during the last glaciation. Quat. Sci. Rev. 201, 280–302. https://doi.org/10.1016/j.quascirev.2018.10.002.

Callard, S.L., Ó Cofaigh, C., Benetti, S., Chiverrell, R.C., Van Landeghem, K.J.J., Saher, M.H., Livingstone, S.J., Clark, C.D., Small, D., Fabel, D., Moreton, S.G., 2020. Oscillating retreat of the last British-Irish Ice Sheet on the continental shelf offshore Galway Bay, western Ireland. Mar. Geol. 420, 106087. https://doi.org/10.1016/j.margeo.2019.106087.

Chiverrell, R.C., Thomas, G.S.P., 2010. Extent and timing of the last glacial maximum (LGM) in britain and Ireland : a review. J. Quat. Sci. 25, 535–549. https://doi.org/10.1002/jqs.1404.

Chiverrell, R.C., Thrasher, I.M., Thomas, G.S.P., Lang, A., Scourse, J.D., van Landeghem, K.J.J., Mccarroll, D., Clark, C.D., Ó Cofaigh, C., Evans, D.J.A., Ballantyne, C.K., 2013. Bayesian modelling the retreat of the Irish sea ice stream. J. Quat. Sci. 28, 200–209. https://doi.org/10.1002/jqs.2616.

Chiverrell, R.C., Smedley, R.K., Small, D., Ballantyne, C.K., Burke, M.J., Callard, S.L., Clark, C.D., Duller, G.A.T., Evans, D.J.A., Fabel, D., Van Landeghem, K.J.J., Livingstone, S., Ó Cofaigh, C., Thomas, G.S.P., Roberts, D.H., Saher, M., Scourse, J.D., Wilson, P., 2018. Ice margin oscillations during deglaciation of the northern Irish Sea Basin. J. Quat. Sci. 33, 739–762. https://doi.org/10.1002/jqs.3057.

Chiverrell, R.C., Thomas, G.S.P., Burke, M., Medialdea, A., Smedley, R., Bateman, M., Clark, C., Duller, G.A.T., Fabel, D., Jenkins, G., Ou, X., Roberts, H.M., Scourse, J., 2020. The evolution of the terrestrial-terminating Irish Sea glacier during the last glaciation. J. Quat. Sci. 36, 752–779. https://doi.org/10.1002/jqs.3229.

Clark, F.E., Patterson, R.T., 1993. An illustrated key to the identification of unilocular genera of calcareous foraminifera. J. Paleontol. 67, 20–28.

Clark, C.D., Knight, J.K., Gray, J.T., 2000. Geomorphological reconstruction of the labrador sector of the Laurentide ice sheet. Quat. Sci. Rev. 19, 1343–1366. https://doi.org/10.1016/S0277-3791(99)00098-0.

Clark, C.D., Hughes, A.L.C., Greenwood, S.L., Spagnolo, M., Ng, F.S.L., 2009a. Size and shape characteristics of drumlins, derived from a large sample, and associated scaling laws. Quat. Sci. Rev. 28, 677–692. https://doi.org/10.1016/j.quascirev.2008.08.035.

Clark, P.U., Dyke, A.S., Shakun, J.D., Carlson, A.E., Clark, J., Wohlfarth, B., Mitrovica, J.X., Hostetler, S.W., McCabe, A.M., 2009b. The last glacial maximum. Science 325 (5941), 710–714. https://doi.org/10.1126/science.1172873.

Clark, C.D., Hughes, A.L.C., Greenwood, S.L., Jordan, C., Petter, H., 2012. Pattern and timing of retreat of the last British-Irish Ice Sheet. Quat. Sci. Rev. 44, 112–146. https://doi.org/10.1016/j.quascirev.2010.07.019.

Clark, G.F., Stark, J.S., Palmer, A.S., Riddle, M.J., Johnston, E.L., 2017. The roles of sea-ice, light and sedimentation in structuring shallow antarctic benthic communities. PLoS One 12, 1–20. https://doi.org/10.1371/journal.pone.0168391.

Clark, C.D., Ely, J.C., Greenwood, S.L., Hughes, A.L.C., Meehan, R., Barr, I.D., Bateman, M.D., Bradwell, T., Doole, J., Evans, D.J.A., Jordan, C.J., Monteys, X., Pellicer, X.M., Sheehy, M., 2018. BRITICE Glacial Map, version 2: a map and GIS database of glacial landforms of the last British–Irish Ice Sheet. Boreas 47, 11–27. https://doi.org/10.1111/bor.12273.

Clark, C.D., Chiverrell, R.C., Fabel, D., Hindmarsh, R.C.A., Ó Cofaigh, C., Scourse, J.D., 2021. Timing, pace and controls on ice sheet retreat: an introduction to the BRITICE-CHRONO transect reconstructions of the British-Irish Ice Sheet. J. Quat. Sci. 36, 673–680. https://doi.org/10.1002/jqs.3326.

Coughlan, M., Tóth, Z., Van Landeghem, K., Mccarron, S., Wheeler, A.J., 2020. Formational history of the Wicklow Trough : a marine-transgressed tunnel valley revealing ice flow velocity and retreat rates for the largest ice stream draining the late-Devensian British-Irish Ice Sheet. J. Quat. Sci. 35, 1–13. https://doi.org/10.1002/jqs.3234.

Davies, D., Bingham, R.G., Graham, A.G.C., Spagnolo, M., Dutrieux, P., Vaughan, D.G., Jenkins, A., Nitsche, F.O., 2017. High-resolution sub-ice-shelf seafloor records of twentieth century ungrounding and retreat of Pine Island Glacier, West Antarctica. J. Geophys. Res. Earth Surf. 122, 1698–1714. https://doi.org/10.1002/2017JF004311.

Davies, B.J., Livingstone, S.J., Roberts, D.H., Evans, D.J.A., Gheorghiu, D.M., Ó Cofaigh, C., 2019. Dynamic ice stream retreat in the central sector of the last British-Irish Ice Sheet. Quat. Sci. Rev. 225, 105989. https://doi.org/10.1016/j.quascirev.2019.105989.

Dove, D., Arosio, R., Finlayson, A., Bradwell, T., Howe, J.A., 2015. Submarine glacial landforms record late Pleistocene ice-sheet dynamics, inner hebrides, scotland. Quat. Sci. Rev. 123, 76–90. https://doi.org/10.1016/j.quascirev.2015.06.012.

Dowdeswell, J.A., Fugelli, E.M.G., 2012. The seismic architecture and geometry of grounding-zone wedges formed at the marine margins of past ice sheets. Bull. Geol. Soc. Am. 124, 1750–1761. https://doi.org/10.1130/B30628.1.

Dowdeswell, J.A., Ottesen, D., Evans, J., Ó Cofaigh, C., Anderson, J.B., 2008. Submarine glacial landforms and rates of ice-stream collapse. Geology 36, 819–822. https://doi.org/10.1130/G24808A.1.

Dowdeswell, J.A., Hogan, K.A., Arnold, N.S., Mugford, R.I., Wells, M., Hirst, J.P.P., Decalf, C., 2015. Sediment-rich meltwater plumes and ice-proximal fans at the margins of modern and ancient tidewater glaciers: observations and modeling. Sedimentology 62, 1665–1692. https://doi.org/10.1111/sed.12198.

Dowdeswell, J.A., Canals, M., Jakobsson, M., Todd, B.J., Dowdeswell, E.K., Hogan, K.A., 2016. The variety and distribution of submarine glacial landforms and implications for ice-sheet reconstruction. In: Atlas of Submarine Glacial Landforms: Modern, Quaternary and Ancient, vol. 46. Geological Society Memoirs, London, pp. 519–552. https://doi.org/10.1144/M46.183.

Dowdeswell, J.A., Batchelor, C.L., Montelli, A., Ottesen, D., Christie, F.D.W., Dowdeswell, E.K., Evans, J., 2020. Delicate seafloor landforms reveal past Antarctic grounding-line retreat of kilometers per year. Science 368 (6494), 1020–1024. https://doi.org/10.1126/science.aaz3059.

Dunlop, P., Shannon, R., McCabe, M., Quinn, R., Doyle, E., 2010. Marine. Geophysical evidence for ice sheet extension and recession on the Malin Shelf: new evidence for the western limits of the British Irish Ice Sheet. Mar. Geol. 276, 86–99. https://doi.org/10.1016/j.margeo.2010.07.010.

Evans, J., Hogan, K.A., 2016. Grounding-zone wedges on the northern larsen shelf, antarctic peninsula. Geol. Soc. Mem. 46, 237–238. https://doi.org/10.1144/M46.3.

Evans, D.J.A., Ó Cofaigh, C., 2003. Depositional evidence for marginal oscillations of the Irish Sea ice stream in southeast Ireland during the last glaciation. Boreas 32, 76–101. https://doi.org/10.1111/j.1502-3885.2003.tb01443.x.

Evans, D.J.A., Phillips, E.R., Hiemstra, J.F., Auton, C.A., 2006. Subglacial till: formation, sedimentary characteristics and classification. Earth Sci. Rev. 78, 115–176. https://doi.org/10.1016/j.earscirev.2006.04.001.

Eyles, N., Eyles, C.H., Miall, A.D., 1983. Lithofacies types and vertical profile models; an alternative approach to the description and environmental interpretation of glacial diamict and diamictite sequences. Sedimentology 30, 393–410. https://doi.org/10.1111/j.1365-3091.1983.tb00679.x.

Farrington, A., 1936. The glaciation of the Bantry Bay district. Proc. R. Irish Acad. 21, 345–361.

Favier, L., Gagliardini, O., Durand, G., Zwinger, T., 2012. A three-dimensional full Stokes model of the grounding line dynamics: effect of a pinning point beneath the ice shelf. Cryosphere 6, 101–112. https://doi.org/10.5194/tc-6-101-2012.

Fisher, R.A., Corbet, A.S., Williams, C.B., 1943. The relation between the number of species and the number of individuals in a random sample of an animal population. J. Anim. Ecol. 12, 42–58. https://doi.org/10.2307/1411.

Furze, M.F.A., Scourse, J.D., Pienkowsky, A.J., Marret, F., Hobbs, W.O., Carter, R.A., Long, B.T., 2014. Deglacial to postglacial palaeoenvironments of the Celtic Sea : lacustrine conditions versus a continuous marine sequence. Boreas 43, 149–174. https://doi.org/10.1111/bor.12028.

Gallagher, C., Thorp, M., 1997. The age of the Pleistocene raised beach near Fethard, County Wexford, using infra red stimulated luminescence (IRSL). Ir. Geogr. 30, 68–89. https://doi.org/10.1080/00750779709478635.

Gallagher, C., Sutton, G., Bell, T., 2004. Submerged ice marginal forms in the Celtic Sea off Waterford harbour. Ireland 37, 145–165. https://doi.org/10.1080/00750770409555839.

García, M., Ercilla, G., Alonso, B., Casas, D., Dowdeswell, J.A., 2011. Sediment lithofacies, processes and sedimentary models in the central bransfield basin, antarctic peninsula, since the last glacial maximum. Mar. Geol. 290, 1–16. https://doi.org/10.1016/j.margeo.2011.10.006.

British Geological Survey, 2013. BGS. Offshore Bedrock Geol. (1250k Scale Map).

Giglio, C., Benetti, S., Sacchetti, F., Lockhart, E., Hughes Clarke, J., Plets, R., Van Landeghem, K., Ó Cofaigh, C., Scourse, J., Dunlop, P., 2021. A Late Pleistocene channelized subglacial meltwater system on the Atlantic continental shelf south of Ireland. Boreas 51 (1), 118–135. https://doi.org/10.1111/bor.12536.

Greenwood, S.L., Clark, C.D., 2008. Subglacial bedforms of the Irish ice sheet. J. Maps 4, 332–357. https://doi.org/10.4113/jom.2008.1030.

Greenwood, S., Simkins, L., Winsborrow, M., Bjarnadottir, L., 2021. Exceptions to bed-controlled ice sheet flow and retreat from glaciated continental margins worldwide. Sci. Adv. 7, 1–13. https://doi.org/10.1130/abs/2020am-350661.

GSI, 2014. Bedrock 1:100 000 https://doi.org/https://www.gsi.ie/en-ie/data-and-maps/Pages/Bedrock.aspx.
Haapaniemi, A.I., Scourse, J.D., Peck, V.L., Kennedy, H., Kennedy, P., Hemming, S.R., Furze, M.F.A., Pienkowski, A.J., Austin, W.E.N., Walden, J., Wadsworth, E., Hall, I.R., 2010. Source, timing, frequency and flux of ice-rafted detritus to the Northeast Atlantic margin, 30-12 ka: testing the Heinrich precursor hypothesis. Boreas 39, 576–591. https://doi.org/10.1111/j.1502-3885.2010.00141.x.
Hald, M., Korsun, S., 1997. Distribution of modern benthic foraminifera from fjords of Svalbard, European Arctic. J. Foraminifer. Res. 27, 101–122. https://doi.org/10.2113/gsjfr.27.2.101.
Hald, M., Steinsund, P.I., Dokken, T., Korsun, S., Polyak, L., Aspeli, R., 1994. Recent and Late Quaternary distribution of Elphidium excavatum f.clavatum in Arctic seas. Cushman Found. Spec. Publ. 32, 141–153.
Hanagata, S., Nobuhara, T., 2015. Illustrated guide to pliocene foraminifera from miyakojima, ryukyu Island arc, with comments on biostratigraphy. Palaeontol. Electron. 18, 1–140. https://doi.org/10.26879/444.
Heaton, T.J., Köhler, P., Butzin, M., Bard, E., Reimer, R.W., Austin, W.E.N., Bronk Ramsey, C., Grootes, P.M., Hughen, K.A., Kromer, B., Reimer, P.J., Adkins, J., Burke, A., Cook, M.S., Olsen, J., Skinner, L.C., 2020. Marine 20—the marine radiocarbon age calibration curve (0–55,000 cal BP). Radiocarbon 62, 779–820. https://doi.org/10.1017/RDC.2020.68.
Hillenbrand, C., Baesler, A., Grobe, H., 2005. The sedimentary record of the last glaciation in the western Bellingshausen Sea (West Antarctica): implications for the interpretation of diamictons in a polar-marine setting. Mar. Geol. 216, 191–204. https://doi.org/10.1016/j.margeo.2005.01.007.
Hillenbrand, C.D., Kuhn, G., Smith, J.A., Gohl, K., Graham, A.G.C., Larter, R.D., Klages, J.P., Downey, R., Moreton, S.G., Forwick, M., Vaughan, D.G., 2013. Grounding-line retreat of the west antarctic ice sheet from inner pine Island Bay. Geology 41, 35–38. https://doi.org/10.1130/G33469.1.
IHO, 2020. International Hydrographic Organization Standards for Hydrographic Surveys S-44. International Hydrographic Organization.
IPCC, 2021. Climate change 2021: the physical science basis, intergovernmental panel on climate change. https://doi.org/10.1080/03736245.2010.480842.
Isarin, R.F.B., 1997. Permafrost distribution and temperatures in europe during the younger Dryas. Permafr. Periglac. Process. 8, 313–333. https://doi.org/10.1002/(SICI)1099-1530(199709)8:3<313::AID-PPP255>3.0.CO;2-E.
Iverson, N.R., McCracken, R.G., Zoet, L.K., Benediktsson, Schomacker, A., Johnson, M.D., Woodard, J., 2017. A theoretical model of drumlin formation based on observations at múlajökull, Iceland. J. Geophys. Res. Earth Surf. 122, 2302–2323. https://doi.org/10.1002/2017JF004354.
Jakobsson, M., Gyllencreutz, R., Mayer, L.A., Dowdeswell, J.A., Canals, M., Todd, B.J., Dowdeswell, E.K., Hogan, K.A., Larter, R.D., 2016. Mapping submarine glacial landforms using acoustic methods. In: Atlas of Submarine Glacial Landforms: Modern, Quaternary and Ancient, vol. 46. Geological Society Memoirs, London, pp. 17–40. https://doi.org/10.1144/M46.182.
Jamieson, S.S.R., Stokes, C.R., Livingstone, S.J., Vieli, A., Ó Cofaigh, C., Hillenbrand, C.D., Spagnolo, M., 2016. Subglacial processes on an Antarctic ice stream bed. 2: can modelled ice dynamics explain the morphology of mega-scale glacial lineations? J. Glaciol. 62, 285–298. https://doi.org/10.1017/jog.2016.19.
Jónsson, S.A., Schomacker, A., Benediktsson, Í.Ö., Ingólfsson, Ó., Johnson, M.D., 2014. The drumlin field and the geomorphology of the Múlajökull surge-type glacier, central Iceland. Geomorphology 207, 213–220. https://doi.org/10.1016/j.geomorph.2013.11.007.
Kilfeather, A.A., Ó Cofaigh, C., Lloyd, J.M., Dowdeswell, J.A., Xu, S., Moreton, S.G., 2011. Ice-stream retreat and ice-shelf history in marguerite trough, antarctic peninsula: sedimentological and foraminiferal signatures. Bull. Geol. Soc. Am. 123, 997–1015. https://doi.org/10.1130/B30282.1.
Kirshner, A.E., Anderson, J.B., Jakobsson, M., O'Regan, M., Majewski, W., Nitsche, F.O., 2012. Post-LGM deglaciation in pine Island Bay, west Antarctica. Quat. Sci. Rev. 38, 11–26. https://doi.org/10.1016/j.quascirev.2012.01.017.
Livingstone, S.J., Clark, C.D., 2016. Morphological properties of tunnel valleys of the southern sector of the Laurentide Ice Sheet and implications for their formation. Earth Surf. Dyn. 4, 567–589. https://doi.org/10.5194/esurf-4-567-2016.
Livingstone, S.J., Ó Cofaigh, C., Evans, D.J.A., 2010. A major ice drainage pathway of the last British–Irish Ice Sheet: the Tyne Gap, northern England. J. Quat. Sci. 25, 354–370. https://doi.org/10.1002/jqs.1341.
Livingstone, S.J., Evans, D.J.A., Ó Cofaigh, C., Davies, B.J., Merritt, J.W., Huddart, D., Mitchell, W.A., Roberts, D.H., Yorke, L., 2012. Glaciodynamics of the central sector of the last British-Irish ice sheet in northern england. Earth Sci. Rev. 111, 25–55. https://doi.org/10.1016/j.earscirev.2011.12.006.
Livingstone, S.J., Stokes, C.R., Ó Cofaigh, C., Hillenbrand, C.D., Vieli, A., Jamieson, S.S.R., Spagnolo, M., Dowdeswell, J.A., 2016. Subglacial processes on an Antarctic ice stream bed. 1: sediment transport and bedform genesis inferred from marine geophysical data. J. Glaciol. 62, 270–284. https://doi.org/10.1017/jog.2016.18.
Lockhart, E.A., Scourse, J.D., Praeg, D., Van Landeghem, K.J.J., Mellett, C., Saher, M., Callard, L., Chiverrell, R.C., Benetti, S., Ó Cofaigh, C., Clark, C.D., 2018. A stratigraphic investigation of the Celtic Sea megaridges based on seismic and core data from the Irish-UK sectors. Quat. Sci. Rev. 198, 156–170. https://doi.org/10.1016/j.quascirev.2018.08.029.
Lønne, I., 1995. Sedimentary facies and depositional architecture of ice-contact glaciomarine systems. Sediment. Geol. 98, 13–43. https://doi.org/10.1016/0037-0738(95)00025-4.
Majewski, W., Prothro, L.O., Simkins, L.M., Demianiuk, E.J., Anderson, J.B., 2020. Foraminiferal patterns in deglacial sediment in the western Ross Sea, Antarctica: life near grounding lines. Paleoceanogr. Paleoclimatol. 35, 1–24. https://doi.org/10.1029/2019PA003716.
McCabe, A.M., 1987. Quaternary deposits and glacial stratigraphy in Ireland. Quat. Sci. Rev. 6, 259–299. https://doi.org/10.1016/0277-3791(87)90008-4.
McCabe, A.M., Eyles, N., 1988. Sedimentology of an ice-contact glaciomarine delta, carey valley, northern Ireland. Sediment. Geol. 59, 1–14. https://doi.org/10.1016/0037-0738(88)90097-8.
McCann, T., Shannon, P.M., 1994. Late mesozoic reactivation of variscan faults in the north Celtic Sea basin, Ireland. Mar. Petrol. Geol. 11, 94–103. https://doi.org/10.1016/0264-8172(94)90012-4.
Menzies, J., 1979. A review of the literature on the formation and location of drumlins. Earth Sci. Rev. 14, 315–359. https://doi.org/10.1016/0012-8252(79)90093-X.
Murray, J.W., 1979. British Nearshore Foraminiferids: Keys and Notes for the Identification of the Species. Academic Press, London.
Murray, J.W., 2003. An illustrated guide to the benthic foraminifera of the hebridean shelf, west of Scotland, with notes on their mode of life. Palaeontol. Electron. 5.
Murray, J.W., 2006. Ecology and applications of benthic foraminifera. Cambridge University Press, Cambridge. https://doi.org/10.1017/CBO9780511535529.
Newton, A.M.W., Huuse, M., 2017. Glacial geomorphology of the central Barents Sea: implications for the dynamic deglaciation of the Barents Sea ice sheet. Mar. Geol. 387, 114–131. https://doi.org/10.1016/j.margeo.2017.04.001.
Ó Cofaigh, C., Dowdeswell, J.A., 2001. Laminated sediments in glacimarine environments: diagnostic criteria for their interpretation. Quat. Sci. Rev. 20, 1411–1436. https://doi.org/10.1016/S0277-3791(00)00177-3.
Ó Cofaigh, C., Evans, D.J.A., 2001a. Deforming bed conditions associated with a major ice stream of the last British ice sheet. Geology 29, 795–798. https://doi.org/10.1130/0091-7613(2001)029<0795:DBCAWA>2.0.CO;2.
Ó Cofaigh, C., Evans, D.J.A., 2001b. Sedimentary evidence for deforming bed conditions associated with a grounded Irish Sea glacier , southern Ireland. J. Quat. Sci. 16, 435–454. https://doi.org/10.1002/jqs.631.
Ó Cofaigh, C., Evans, D.J.A., 2007. Radiocarbon constraints on the age of the maximum advance of the British – Irish ice sheet in the Celtic Sea. Quat. Sci. Rev. 26, 1197–1203. https://doi.org/10.1016/j.quascirev.2007.03.008.
Ó Cofaigh, C., Dowdeswell, J.A., Allen, C.S., Hiemstra, J.F., Pudsey, J., Evans, J., Evans, D.J.A., 2005. Flow dynamics and till genesis associated with a marine-based Antarctic palaeo-ice stream. Quat. Sci. Rev. 24, 709–740. https://doi.org/10.1016/j.quascirev.2004.10.006.
Ó Cofaigh, C., Evans, J., Dowdeswell, J.A., Larter, R.D., 2007. Till characteristics, genesis and transport beneath Antarctic paleo-ice streams. J. Geophys. Res. Earth Surf. 112, 1–16. https://doi.org/10.1029/2006JF000606.
Ó Cofaigh, C., Evans, D.J.A., Hiemstra, J., 2008. Till sedimentology and stratigraphy on the Dingle Peninsula, SW Ireland: implications for Late Quaternary regional ice flow patterns. Proc. Geol. Assoc. 119, 137–152. https://doi.org/10.1016/S0016-7878(08)80314-8.
Ó Cofaigh, C., Telfer, M.W., Bailey, R.M., Evans, D.J.A., 2012a. Late Pleistocene chronostratigraphy and ice sheet limits , southern Ireland. Quat. Sci. Rev. 44, 160–179. https://doi.org/10.1016/j.quascirev.2010.01.011.
Ó Cofaigh, C., Dunlop, P., Benetti, S., 2012b. Marine geophysical evidence for Late Pleistocene ice sheet extent and recession off northwest Ireland. Quat. Sci. Rev. 44, 147–159. https://doi.org/10.1016/j.quascirev.2010.02.005.
Ó Cofaigh, C., Weilbach, K., Lloyd, J.M., Benetti, S., Callard, S.L., Purcell, C., Chiverrell, R.C., Dunlop, P., Saher, M., Livingstone, S.J., Van Landeghem, K.J.J., Moreton, S.G., Clark, C.D., Fabel, D., 2019. Early deglaciation of the British-Irish Ice Sheet on the Atlantic shelf northwest of Ireland driven by glacioisostatic depression and high relative sea level. Quat. Sci. Rev. 208, 76–96. https://doi.org/10.1016/j.quascirev.2018.12.022.
Ó Cofaigh, C., Callard, S.L., Roberts, D.H., Chiverrell, R.C., Ballantyne, C.K., Evans, D.J.A., Saher, M., Van Landeghem, K.J.J., Smedley, R., Benetti, S., Burke, M., Clark, C.D., Duller, G.A.T., Fabel, D., Livingstone, S.J., Mccarron, S., Medialdea, A., Moreton, S.G., Sacchetti, F., 2021. Timing and pace of ice-sheet withdrawal across the marine-terrestrial transition west of Ireland during the last glaciation. J. Quat. Sci. 36, 805–832. https://doi.org/10.1002/jqs.3295.
Ottesen, D., Dowdeswell, J.A., Rise, L., 2005. Submarine landforms and the reconstruction of fast-flowing ice streams within a large Quaternary ice sheet: the 2500-km-long Norwegian-Svalbard margin (57°-80°N). Bull. Geol. Soc. Am. 117, 1033–1050. https://doi.org/10.1130/B25577.1.
Ottesen, D., Dowdeswell, J.A., Bellec, V.K., Bjarnadóttir, L.R., 2017. The geomorphic imprint of glacier surges into open-marine waters: examples from eastern Svalbard. Mar. Geol. 392, 1–29. https://doi.org/10.1016/j.margeo.2017.08.007.
Pantin, H., Evans, C.D.R., 1984. The Quaternary history of the central and south-western Celtic Sea. Mar. Geol. 57, 259–293. https://doi.org/10.1016/0025-3227(84)90202-0.
Peters, J.L., Benetti, S., Dunlop, P., Ó Cofaigh, C., Moreton, S.G., Wheeler, A.J., Clark, C.D., 2016. Sedimentology and chronology of the advance and retreat of the last British-Irish Ice Sheet on the continental shelf west of Ireland. Quat. Sci. Rev. 140, 101–124. https://doi.org/10.1016/j.quascirev.2016.03.012.
Peters, J.L., Benetti, S., Dunlop, P., Wheeler, A.J., 2020. Sedimentary and foraminiferal records of Late Quaternary environmental change west of Ireland and implications for the last British–Irish Ice Sheet. J. Quat. Sci. 35, 609–624. https://doi.org/10.1002/jqs.3208.
Plets, R.M.K., Callard, S.L., Cooper, J.A.G., Long, A.J., Quinn, R.J., Belknap, D.F., Edwards, R.J., Jackson, D.W.T., Kelley, J.T., Long, D., Milne, G.A., Monteys, X., 2015. Late Quaternary evolution and sea-level history of a glaciated marine

embayment, Bantry Bay, SW Ireland. Mar. Geol. 369, 251–272. https://doi.org/10.1016/j.margeo.2015.08.021.
Plets, R.M.K., Callard, S.L., Cooper, J.A.G., Kelley, J.T., Belknap, D.F., Edwards, R.J., Long, A.J., Quinn, R.J., Jackson, D.W.T., 2019. Late Quaternary sea-level change and evolution of Belfast Lough, Northern Ireland: new offshore evidence and implications for sea-level reconstruction. J. Quat. Sci. 34, 285–298. https://doi.org/10.1002/jqs.3100.
Powell, R.D., 1990. Glacimarine processes at grounding-line fans and their growth to ice-contact deltas. Geol. Soc. London, Spec. Publ. 53, 53–73. https://doi.org/10.1144/GSL.SP.1990.053.01.03.
Powell, R.D., Alley, R.B., 1997. Grounding-line systems: processes, glaciological inferences and the stratigraphic record. Antarct. Res. 71, 169–187. https://doi.org/10.1029/ar071p0169.
Praeg, D., McCarron, S., Dove, D., Ó Cofaigh, C., Scott, G., Monteys, X., Facchin, L., Romeo, R., Coxon, P., 2015. Ice sheet extension to the Celtic Sea shelf edge at the last glacial maximum. Quat. Sci. Rev. 111, 107–112. https://doi.org/10.1016/j.quascirev.2014.12.010.
Pratch, M., Sleeman, A., 2002. Geology of West Cork, Map Series.
Price, S.F., Payne, A.J., Howat, I.M., Smith, B.E., 2011. Committed sea-level rise for the next century from Greenland ice sheet dynamics during the past decade. Proc. Natl. Acad. Sci. U.S.A. 108, 8978–8983. https://doi.org/10.1073/pnas.1017313108.
Prothro, L.O., Simkins, L.M., Majewski, W., Anderson, J.B., 2018. Glacial retreat patterns and processes determined from integrated sedimentology and geomorphology records. Mar. Geol. 395, 104–119. https://doi.org/10.1016/j.margeo.2017.09.012.
Rasmussen, S.O., Andersen, K.K., Svensson, A.M., Steffensen, J.P., Vinther, B.M., Clausen, H.B., Siggaard-Andersen, M.L., Johnsen, S.J., Larsen, L.B., Dahl-Jensen, D., Bigler, M., Röthlisberger, R., Fischer, H., Goto-Azuma, K., Hansson, M.E., Ruth, U., 2006. A new Greenland ice core chronology for the last glacial termination. J. Geophys. Res. Atmos. 111, 1–16. https://doi.org/10.1029/2005JD006079.
Rignot, E., Mouginot, J., Scheuchl, B., 2011. Ice flow of the antarctic ice sheet. Science 333 (6048), 1427–1430. https://doi.org/10.1126/science.1208336.
Rust, B.R., Romanelli, R., 1975. Late Quaternary subaqueous outwash deposits near Ottawa, Canada. In: Glaciofluvial and Glaciolacustrine Sedimentation. SEPM (Society for Sedimentary Geology), pp. 177–192. https://doi.org/10.2110/pec.75.23.0177.
Schomacker, A., 2011. Moraine. In: Singh, V.P., Singh, P., Haritashya, U.K. (Eds.), Encyclopedia of Snow, Ice and Glaciers. Springer, pp. 747–755.
Scourse, J.D., Furze, M.F.A., 2001. A critical review of the glaciomarine model for Irish sea deglaciation : evidence from southern Britain, the Celtic shelf and adjacent continental slope. J. Quat. Sci. 16, 419–434. https://doi.org/10.1002/jqs.629.
Scourse, J.D., Austin, W.E.N., Bateman, R.M., Catt, J.A., Evans, C.D.R., Robinson, J.E., Young, J.R., 1990. Sedimentology and micropalaeontology of glacimarine sediments from the central and southwestern Celtic Sea. Geol. Soc. London, Spec. Publ. 53, 329–347. https://doi.org/10.1144/GSL.SP.1990.053.01.19.
Scourse, J.D., Austin, W.E.N., Long, B.T., Assinder, D.J., Huws, D., 2002. Holocene evolution of seasonal stratification in the Celtic Sea: refined age model, mixing depths and foraminiferal stratigraphy. Mar. Geol. 191, 119–145. https://doi.org/10.1016/S0025-3227(02)00528-5.
Scourse, J.D., Haapaniemi, A.I., Colmenero-hidalgo, E., Peck, V.L., Hall, I.R., Austin, W.E.N., Knutz, P.C., Zahn, R., 2009. Growth , dynamics and deglaciation of the last British – Irish ice sheet : the deep-sea ice-rafted detritus record. Quat. Sci. Rev. 28, 3066–3084. https://doi.org/10.1016/j.quascirev.2009.08.009.
Scourse, J.D., Saher, M., Van Landeghem, K.J.J., Lockhart, E., Purcell, C., Callard, L., Roseby, Z., Allinson, B., Pieńkowski, A.J., Ó Cofaigh, C., Praeg, D., Ward, S., Chiverrell, R., Moreton, S., Fabel, D., Clark, C.D., 2019. Advance and retreat of the marine-terminating Irish sea ice stream into the Celtic Sea during the last glacial: timing and maximum extent. Mar. Geol. 412, 53–68. https://doi.org/10.1016/j.margeo.2019.03.003.
Scourse, J.D., Chiverrell, R.C., Smedley, R.K., Small, D., Burke, M.J., Saher, M., Van Landeghem, K.J.J., Duller, G.A.T., Ó Cofaigh, C., Bateman, M.D., Benetti, S., Bradley, S., Callard, L., Evans, D.J.A., Fabel, D., Jenkins, G.T.H., McCarron, S., Medialdea, A., Moreton, S., Ou, X., Praeg, D., Roberts, D.H., Roberts, H.M., Clark, C.D., 2021. Maximum extent and readvance dynamics of the Irish sea ice stream and Irish sea glacier since the last glacial maximum. J. Quat. Sci. 36, 780–804. https://doi.org/10.1002/jqs.3313.
Shaw, J., Piper, D.J.W., Fader, G.B.J., King, E.L., Todd, B.J., Bell, T., Batterson, M.J., Liverman, D.G.E., 2006. A conceptual model of the deglaciation of Atlantic Canada. Quat. Sci. Rev. 25, 2059–2081. https://doi.org/10.1016/j.quascirev.2006.03.002.
Shipp, S.S., Wellner, J.S., Anderson, J.B., 2002. Retreat signature of a polar ice stream: sub-glacial geomorphic features and sediments from the Ross Sea, Antarctica. Geol. Soc. Spec. Publ. 203, 277–304. https://doi.org/10.1144/GSL.SP.2002.203.01.15.
Simkins, L.M., Greenwood, S.L., Anderson, J.B., 2018. Diagnosing ice sheet grounding line stability from landform morphology. Cryosphere 12, 2707–2726. https://doi.org/10.5194/tc-12-2707-2018.
Small, D., Smedley, R.K., Chiverrell, R.C., Scourse, J.D., Ó Cofaigh, C., Duller, G.A.T., Mccarron, S., Burke, M.J., Evans, D.J.A., Fabel, D., Gheorghiu, D.M., Thomas, G.S.P., Xu, S., Clark, C.D., 2018. Trough geometry was a greater influence than climate-ocean forcing in regulating retreat of the marine-based Irish-Sea Ice Stream. GSA Bull 130, 1981–1999. https://doi.org/10.1130/B31852.1.
Smedley, R.K., Chiverrell, R.C., Ballantyne, C.K., Burke, M.J., Clark, C.D., Duller, G.A.T., Fabel, D., Mccarroll, D., Scourse, J.D., Small, D., Thomas, G.S.P., 2017a. Internal dynamics condition centennial-scale oscillations in marine- based ice-stream retreat. Geology 45, 787–790. https://doi.org/10.1130/G38991.1.
Smedley, R.K., Scourse, J.D., Small, D., Hiemstra, J.F., Duller, G.A.T., Bateman, M.D., Burke, M.J., Chiverrell, R.C., Clark, C.D., Davies, S.M., Fabel, D., Gheorghiu, D.M., McCarroll, D., Medialdea, A., Xu, S., 2017b. New age constraints for the limit of the British – Irish ice sheet on the Isles of scilly. J. Quat. Sci. 32, 48–62. https://doi.org/10.1002/jqs.2922.
Smith, L.M., Andrews, J.T., 2000. Sediment characteristics in iceberg dominated fjords, Kangerlussuaq region, East Greenland. Sediment. Geol. 130, 11–25. https://doi.org/10.1016/S0037-0738(99)00088-3.
Smith, A.M., Murray, T., Nicholls, K.W., Makinson, K., Adalgeirsdóttir, G., Behar, A.E., Vaughan, D.G., 2007. Rapid erosion, drumlin formation, and changing hydrology beneath an Antarctic ice stream. Geology 35, 127–130. https://doi.org/10.1130/G23036A.1.
Smith, B., Fricker, H.A., Gardner, A.S., Medley, B., Nilsson, J., Paolo, F.S., Holschuh, N., Adusumilli, S., Brunt, K., Csatho, B., Harbeck, K., Markus, T., Neumann, T., Siegfried, M.R., Zwally, H.J., 2020. Pervasive ice sheet mass loss reflects competing ocean and atmosphere processes. Science 368 (6496), 1239–1242. https://doi.org/10.1126/science.aaz5845.
Sookhan, S., Eyles, N., Bukhari, S., Paulen, R.C., 2021. LiDAR-based quantitative assessment of drumlin to mega-scale glacial lineation continuums and flow of the paleo Seneca-Cayuga paleo-ice stream. Quat. Sci. Rev. 263, 107003. https://doi.org/10.1016/j.quascirev.2021.107003.
Stokes, C.R., 2018. Geomorphology under ice streams: moving from form to process. Earth Surf. Process. Landforms 43, 85–123. https://doi.org/10.1002/esp.4259.
Stokes, C.R., Tarasov, L., Blomdin, R., Cronin, T.M., Heyman, J., Fisher, T.G., Gyllencreutz, R., Clas, H., Hindmarsh, R.C.A., Hughes, A.L.C., Jakobsson, M., Kirchner, N., Livingstone, S.J., Margold, M., Murton, J.B., Noormets, R., Peltier, W.R., Peteet, D.M., Piper, D.J.W., Preusser, F., Renssen, H., Roberts, D.H., Roche, D.M., Saint-Ange, F., Stroeven, A.P., Teller, J.T., 2015. On the reconstruction of palaeo-ice sheets : recent advances and future challenges. Quat. Sci. Rev. 125, 15–49. https://doi.org/10.1016/j.quascirev.2015.07.016.
Stow, D.A.V., Hernández-Molina, F.J., Llave, E., Sayago-Gil, M., Díaz-del Río, V., Branson, A., 2009. Bedform-velocity matrix: the estimation of bottom current velocity from bedform observations. Geology 37, 327–330. https://doi.org/10.1130/G25259A.1.
Syvitski, J.P.M., 1991. Towards an understanding of sediment deposition on glaciated continental shelves. Continent. Shelf Res. 11, 897–937. https://doi.org/10.1016/0278-4343(91)90085-K.
Szuman, I., Kalita, J.Z., Ewertowski, M.W., Clark, C.D., Livingstone, S.J., 2021a. Dynamics of the last Scandinavian Ice Sheet's southernmost sector revealed by the pattern of ice streams. Boreas 50, 764–780. https://doi.org/10.1111/bor.12512.
Szuman, I., Kalita, J.Z., Ewertowski, M.W., Clark, C.D., Livingstone, S.J., Kasprzak, L., 2021b. GIS dataset: geomorphological record of terrestrial-terminating ice streams, southern sector of the Baltic Ice Stream Complex, last Scandinavian Ice Sheet, Poland. Earth Syst. Sci. Data 13, 4635–4651. https://doi.org/10.5194/essd-13-4635-2021.
Tóth, Z., McCarron, S., Wheeler, A.J., Wenau, S., Davis, S., Lim, A., Spiess, V., 2020. Geomorphological and seismostratigraphic evidence for multidirectional polyphase glaciation of the northern Celtic Sea. J. Quat. Sci. 35, 465–478. https://doi.org/10.1002/jqs.3189.
van der Meer, J.J.M., Verbers, A.L.L.M., Warren, W.P., 1994. The Micromorphological Character of the Ballycroneen Formation (Irish Sea till): a First Assessment, Formation and Deformation of Glacial Deposits, ISBN 90 5410 096 6.
Van Landeghem, K.J.J., Chiverrell, R.C., 2020. Bed erosion during fast ice streaming regulated the retreat dynamics of the Irish Sea Ice Stream. Quat. Sci. Rev. 245, 106526. https://doi.org/10.1016/j.quascirev.2020.106526.
Van Rooij, D., 2004. An Integrated Study of Quaternary Sedimentary Processes on the Eastern Slope of the Porcupine Seabight, SW of Ireland. Ghent University.
Vaughan, D.G., Arthern, R., 2007. Why is it hard to predict the future of ice sheets? Science 315 (5818), 1503–1504. https://doi.org/10.1126/science.1141111.
Viana, A.R., Faugères, J.C., Stow, D.A.V., 1998. Bottom-current-controlled sand deposits — a review of modern shallow- to deep-water environments. Sediment. Geol. 115, 53–80. https://doi.org/10.1016/S0037-0738(97)00087-0.
Warren, W.P., 1991. Glacial deposits of southwest Ireland. In: Ehlers, J., Gibbard, P.L., Rose, J., Denton, G.H. (Eds.), Glacial Deposits of Great Britain and Ireland, pp. 345–353. Rotterdam.
Weilbach, K., 2018. Extent, Timing and Nature of Retreat of the British-Irish Ice Sheet Offshore of North-Western Ireland during and Following the Last Glacial Maximum. Unpublished PhD Thesis. Durham University. https://doi.org/http://etheses.dur.ac.uk/12655/.
Winsborrow, M.C.M., Clark, C.D., Stokes, C.R., 2010. What controls the location of ice streams? Earth Sci. Rev. 103, 45–59. https://doi.org/10.1016/j.earscirev.2010.07.003.
Wood, B.L., Williams, D.M., Murray, J., 2018. Effects of the Younger Dryas climate event recorded in sediment near the western Irish seaboard. Geol. J. 53, 647–659. https://doi.org/10.1002/gj.2918.
Wood, M., Rignot, E., Fenty, I., An, L., Bjørk, A., van den Broeke, M., Cai, C., Kane, E., Menemenlis, D., Millan, R., Morlighem, M., Mouginot, J., Noël, B., Scheuchl, B., Velicogna, I., Willis, J.K., Zhang, H., 2021. Ocean forcing drives glacier retreat in Greenland. Sci. Adv. 7, 1–11. https://doi.org/10.1126/sciadv.aba7282.
Wright, W.B., Muff, H.B., 1904. The pre-glacial raised beach of the south coast of Ireland. Irish Nat 13, 291–294.